# FEW-ELECTRON QUANTUM DOT MOLECULES

Meri Helle

*Laboratory of Physics*
*Helsinki University of Technology*
*Espoo, Finland*

Dissertation for the degree of Doctor of Science in Technology to be presented with due permission of the Department of Engineering Physics and Mathematics for public examination and debate in Auditorium E at Helsinki University of Technology (Espoo, Finland) on the 5th of January, 2006, at 12 o'clock noon.

*Helsinki University of Technology*
*Department of Engineering Physics and Mathematics*
*Laboratory of Physics*
*P.O.Box 1100*
*FI-02015 TKK, Finland*
*URL: http://www.fyslab.hut.fi/*
*Tel. +358-9-4513101*
*Meri.Helle@iki.fi*

*Dissertations of Laboratory of Physics, Helsinki University of Technology*
*ISSN 1455-1802*
*Dissertation 137 (2005):*
*Meri Helle: Few-electron quantum dot molecules*
*ISBN 951-22-7985-1 (print)*
*ISBN 951-22-7986-X (electronic)*
*URL: http://lib.tkk.fi/Diss/2006/isbn951227986X/*

Picaset Oy
Helsinki 2005

| HELSINKI UNIVERSITY OF TECHNOLOGY<br>P. O. BOX 1000, FI-02015 TKK<br>http://www.tkk.fi | ABSTRACT OF DOCTORAL DISSERTATION |
|---|---|

Author Meri Helle

Name of the dissertation

Few-electron quantum-dot molecules

| Date of manuscript December 12, 2005 | Date of the dissertation January 5, 2006 |
|---|---|

☐ Monograph ☒ Article dissertation (summary + original articles)

| | |
|---|---|
| Department | Engineering Physics and Mathematics |
| Laboratory | Laboratory of Physics |
| Field of research | Computational Physics |
| Opponent(s) | Professor Francois Peeters, University of Antwerp |
| Supervisor | Academy Professor Risto Nieminen, Helsinki University of Technology |
| (Instructor) | Docent Ari Harju, Helsinki University of Technology |

Abstract

Semiconductor quantum dots have been studied for nearly two decades with a variety of experimental and theoretical methods. The typical dimensions of these “artificial atoms” are from a hundred nanometers to one micrometer and the number of electrons inside the quantum dots can range from one to several hundred. The tunable size, shape and electron number, as well as the enhanced electron correlation and magnetic field effects, makes quantum dots excellent objects for studying fascinating many-electron quantum physics in a controlled way. In the rapidly growing fields of nanoscience and nanotechnology, quantum dots are promising candidates for future nanoelectronic devices. One of the most intriguing scenarios of quantum dot applications lies in the utilization of an electron spin as a quantum bit in quantum computing.

This Thesis deals with the modeling of electron states in two-dimensional coupled quantum dots or quantum-dot molecules. The emphasis is on describing electron correlations properly but concentrating only on a few electrons inside the quantum-dot molecules. In this Thesis we mostly consider two interacting electrons and find remarkably complex behavior as a function of the magnetic field. We find the electron-electron interactions and the shape of the confining potential to have a profound effect on the two-electron quantum states.

The main results of this Thesis are the calculations and analysis of the quantum-mechanical states of two electrons in a magnetic field. This includes the ground-state transitions and magnetizations of the system as a function of magnetic field and careful analysis of the wave functions and the calculation and analysis of the far-infrared magneto-optical absorption spectra. We also study classical electrons in a quantum-dot molecule. This is relevant for the Wigner crystallization of electrons in a very high magnetic field or in a very low electron density.

Keywords semiconductor quantum dots, magnetic field, far-infrared absorption, exact diagonalization

| | |
|---|---|
| ISBN (printed) 951-22-7985-1 | ISSN (printed) 1455-1802, dissertation 137 |
| ISBN (pdf) 951-22-7986-X | ISSN (pdf) |
| ISBN (others) | Number of pages 62 p. + app. 70 p. |

Publisher Laboratory of Physics, Helsinki University of Technology

Print distribution Laboratory of Physics, Helsinki University of Technology

☒ The dissertation can be read at http://lib.tkk.fi/Diss/2006/isbn951227986X/

# Preface

This Thesis has been prepared in the Computational Condensed Matter and Complex Materials Group (COMP) of the Laboratory of Physics at the Helsinki University of Technology (TKK) during the years 2001-2005. I have had a pleasure to get to know many fine colleagues and students at TKK and from other universities during my postgraduate studies to whom I wish to express my warmest thanks for many nice discussions and moments.

I am particularly grateful to my supervisor Academy Professor Risto Nieminen for his scientific contribution and supervision. I appreciate Prof. Nieminen's advice and guidance during my years in the group. Although Prof. Nieminen has been a busy group leader of the COMP group, he has always found time for discussions. I am indebted to my instructor Dr. Ari Harju whose contribution to the thesis has been considerable in the scientific part but also in the practical matters. Many of the research subjects were initiated by Ari and my disordered thoughts were greatly refined by Ari. I would also like to thank Professor Matti Alatalo for his contribution.

Special thanks go to Dr. Sami Siljamäki, former graduate student at TKK, who provided the subgroup with a cheerful atmosphere. I have greatly valued our discussions on the realm of science and life. I am also grateful to other "Nabel discussion group" members, Dr. Ari Harju, Dr. Esa Räsänen, Dr. Henri Saarikoski, Dr. Paula Havu, M.Sc. Sigrídur (Sigga) Sif Gylfadóttir and Juha Suorsa for scientific and non-scientific discussions along with their great company. Especially I want to say to Sigga that it has been a pleasure to share an office with you. I would also like to mention some present and past members of Lab. of Physics, with many of whom I have shared teaching responsibilities. I thank M.Sc. Emma Terämä, M.Sc. Katri Laaksonen, Dr. Juha Lento, Dr. Petri Salo and Eija Järvinen for contributing to the nice working environment. I also wish to extend my thanks to all other Lab. of Physics members even if their names are not mentioned here.

The financial support from the Väisälä Foundation, the Finnish Cultural Foundation, the Magnus Ehrnrooth Foundation, and the Jenny and Antti Wihuri Foundation is gratefully acknowledged.

I want to thank my family and friends for all the support and caring during this thesis work. Finally, my warmest thanks go to my dear husband Jaakko.

Helsinki, December 2005

*Meri Helle*

## List of publications

This Thesis consists of an overview and the following publications:

**I** M. Marlo, M. Alatalo, A. Harju, and R. M. Nieminen, *Lateral diatomic two-dimensional artificial molecules: Classical transitions and quantum-mechanical counterparts*, Physical Review B **66**, 155322 (2002) (7 pages).

**II** M. Marlo, A. Harju, and R. M. Nieminen, *Role of interactions in the far-infrared spectrum of a quantum-dot molecule*, Physical Review Letters **91**, 187401 (2003) (4 pages).

**III** M. Marlo-Helle, A. Harju, and R. M. Nieminen, *Singlet-triplet oscillations and far-infrared spectra in four-minima quantum-dot molecules*, Physica E **26**, 286 (2005) (5 pages).

**IV** M. Helle, A. Harju, and R. M. Nieminen, *Two-electron lateral quantum-dot molecules in a magnetic field*, Physical Review B **72**, 205329 (2005) (24 pages).

**V** M. Helle, A. Harju, and R. M. Nieminen, *Far-infrared spectra of lateral quantum-dot molecules*, submitted to New Journal of Physics (2005) (17 pages), cond-mat/0511577.

The author Meri Helle (prev. Marlo) has had an active role in all the phases of the research reported in this Thesis. The author has had the main responsibility of the calculations and the scientific analysis of the results presented in the publications. The author has chosen the computational approach and written the necessary computer programs for the results reported in Publication **I**. She has contributed to the modifications of the computer program employed to calculate the results presented in Publications **II-V**. She has written the main drafts of all the publications.

# Contents

# Chapter 1

# Introduction

The last decades have shown a rapid increase of the information processing power of computers. Progress in manufacturing techniques have enabled sub-micron semiconductor device sizes and the production of faster computer processors. As the single device dimension in the semiconductor chips approaches the nanometer length scale, quantum mechanical effects become relevant to the device functioning. This raises challenges for existing technologies but at the same time opportunities for future nanoelectronics. One of the most interesting prospects lies in the endeavors of building a quantum computer from the nano-sized semiconductor devices.

Semiconductor quantum dots or "artificial atoms" are man-made devices in which electrons are confined into a nanoscale volume. Electrons in a quantum dot device can be controlled with electrodes and magnetic fields. Two-dimensional semiconductor quantum dots are typically fabricated in the semiconductor heterostructures using lithographic techniques. They are manufactured in research laboratories, and measurements are performed at very low temperatures. The peculiar quantum behavior of electrons in quantum dots is under investigation in many laboratories around the world. The tunable size, shape and electron number, as well as the enhanced electron correlation and magnetic field effects, makes quantum dots excellent objects for studying fascinating many-electron quantum physics in a controlled way.

This Thesis deals with the modeling of electron states in coupled quantum dots or quantum-dot molecules. The properties of a single quantum-mechanical electron in a quantum dot can be described with a good accuracy, but for many electrons, the interaction between the electrons converts the quantum-mechanical problem into very complicated. We have chosen to use a very accurate, but computationally heavy, exact diagonalization method for modeling the electrons confined in quantum-dot molecules. We describe just a few electrons, mainly

two, inside the quantum-dot molecules. This is motivated by two aspects: Interacting quantum-mechanical electrons may produce the most peculiar states such as the ones found in the fractional quantum Hall effect where more approximative mean-field methods cannot always provide the correct physical picture. Also many experimental studies have been exploring one- and two-electron states in coupled quantum dots, motivated by the idea of using electron spins in quantum computing. In this Thesis we analyse the effects of electron correlations and quantum-dot molecule confinement potential on energy levels, magnetization and far-infrared magneto-optical absorption spectra, as well as the effects on the wave function structure of the quantum-dot molecules. The objective of this Thesis is to characterize and understand the physical phenomena of many-electron states in quantum-dot molecules.

This Thesis is organized as follows. Chapter 2 represents properties of semiconductor quantum dots and experimental methods, including a brief review of the current research on the topic. Chapter 3 deals with the theoretical description of a single quantum-mechanical electron in a semiconductor quantum dot or in a quantum-dot molecule. In addition, the basic requirements for many-electron states are discussed. Chapter 4 introduces the exact diagonalization method, the computational approach used in this Thesis, beginning with the matrix formulation of quantum mechanics, and continuing with the calculation of the matrix elements of the Hamiltonian matrix for quantum-dot molecules. The diagonalization method is also discussed from the perspective of other computational approaches. Some of the results of the Thesis are briefly summarized in Chapter 5. A more detailed discussion can be found in the Publications **I**-**V**. In Chapter 5 we first discuss ground state transitions of the spin-singlet and spin-triplet states as a function of magnetic field, and also the magnetization curves, as well as the low-lying energy states of the quantum-dot molecules. These experimentally measurable quantities are followed by the analysis of the wave function structures of the quantum-dot molecules in a magnetic field. Thereafter, we discuss far-infrared absorption spectra of quantum-dot molecules, studied in the Publications **II**, **III** and **V**. Finally, transitions in classical electron configurations and their quantum-mechanical counterparts are briefly presented, referring to Publication **I** for more detailed discussion. A summary of the Thesis is given in Chapter 6.

# Chapter 2

# Quantum dots

The progress in semiconductor technology has enabled the production of very small-scale devices where a controllable number of electrons are confined into a small volume. These man-made structures are usually called artificial atoms or quantum dots [1–4]. Quantum dots with different sizes and properties can be produced, and the number of electrons in the dot can be changed by external gate electrodes.

The artificial atoms differ from real atoms in two respects: in quantum dots the electrons are usually confined to a much larger volume than the electrons in a real atom. In addition, the shape of the confining potential in the quantum dots is quite different from the one in a real atom. Typically a quantum dot structure resembles a two-dimensional box with a side length of $\sim$ 100 nm whereas in the solids the spacing between the atoms is of the order of a few Ångströms ($\sim 0.2 - 0.3$ nm). A single semiconductor quantum dot consists of the order of $10^6$ atoms. Most of the electrons in the material are bound to atoms but some of the electrons can be made to move freely in the quantum dot region. The other difference, besides the huge size difference, between real atoms and quantum dots is in the form of the potential. In real atoms the strong Coulomb attraction of the nucleus restricts the electron motion into a small volume in the proximity of the nucleus. In quantum dots the potential is not a central attractive, but resembles more a harmonic trap defined by the external electrodes (lateral quantum dot) or by the physical dimensions (vertical quantum dot). Yet another interesting feature is that there exists a class of semiconductor quantum dots that can be considered effectively two-dimensional which gives rise to some fascinating physics as well.

As the size and the shape of the confinement potential differs from real atoms, also the energy scales are modified in quantum dots. Even if electrons are free to move in a quantum dot, the mass of electrons is different from a free electron

mass due to the surrounding host semiconductor material. Usually the electrons in the quantum dot devices can be described with an effective-mass approximation. Because of these differences, the Coulomb and magnetic field effects are very much enhanced in quantum dots compared to real atoms. This leads to intriguing many-electron and magnetic field effects that can be studied in a controlled way by changing the gate electrode voltages and the magnetic field strength. The semiconductor quantum dots, considered in this Thesis, are effectively two-dimensional and therefore quantum Hall states could be observed at high magnetic fields [5]. However, quantum dots are tiny objects compared to the two-dimensional electron gas in the quantum Hall systems. Actually, it is an interesting question how the quantized energy levels affect the states at high magnetic fields [6–8]. In fact, recent experiments suggest that also integer quantum Hall states might be much more complicated than was believed in the past [9]. Maybe future experiments and theories of large quantum dots at high magnetic fields are able to shed light on the nature of quantum Hall states [7, 8, 10]. Also quantum shot noise measurements could reveal some interesting properties of quantum states inside nanoscale quantum dots [11, 12]. Another interesting research direction in the field of two-dimensional semiconductor quantum dots has been the coupling of two or more quantum dots together, thus going from single quantum dots to quantum-dot molecules [13–18].

Coupled quantum dots have also drawn great interest recently in the context of quantum computing [19]. It has turned out that electron spins in quantum dots are good candidates for qubits (quantum bits) [20–22]. The last couple of years have speeded up a number of experimental efforts to fulfill the requirements for a realizable quantum computer [23] which would require the following steps: *i*) isolate single electrons in individual quantum dots, *ii*) initialize the state in the beginning of the computation, *iii*) isolate qubits from the environment, *iv*) perform quantum gate operations and *v*) read out the qubit [24, 25]. While the number of qubits required for useful quantum computations is around $10^5$, the experiments have been struggling with initializing, characterizing, and reading the single- and two-qubit states [26–35]. Remarkably, during this year the coherent manipulation of two-spin system was realized for the very first time [36, 37]. Even if the achievements seem rather modest from the point of view of realistic quantum computing, the measurements are great accomplishments in understanding few-electron quantum physics. Single-electron or single-spin controlling is far from an easy task. Knowledge of the operations of these entangled few-electron nanocircuits may also be useful in other applications, not to mention the scientific interest in understanding the behavior of few-electron quantum states.

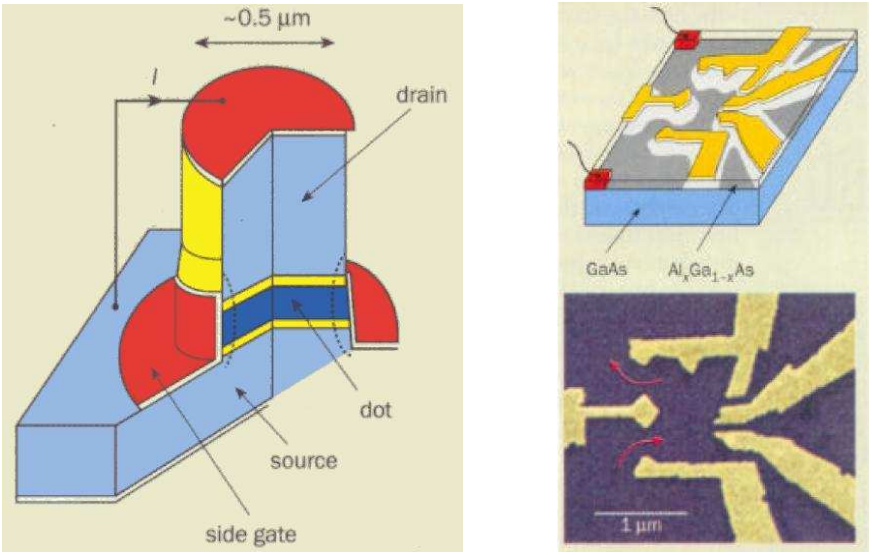


Figure 2.1: Schematic picture of a vertical quantum dot (left) and a lateral quantum dot (right upper). The lower right panel shows a scanning electron micrograph of a lateral quantum dot. (Adapted from Ref. [3] by Kouwenhoven and Marcus).

## 2.1 Fabrication and properties of quantum dots

A quantum dot is an artificially produced structure where electrons are localized into a small spatial volume. One way to produce a quantum dot is to isolate a small piece of metal with insulating material, for example to grow a small island of metal on an insulating substrate (*e.g.* Al island on Si). Metallic quantum dots tend to be rather large and the energy levels lie close to each other, thus approaching the continuum limit. More commonly studied few-electron quantum dots are fabricated in the two-dimensional electron gas (2DEG) in a semiconductor heterostructure. High quality 2DEG is typically created in a modulation doped GaAs-AlGaAs heterostructure which leads to high electron-mobility 2DEG in the GaAs side near the interface of the two semiconductors. Confinement in two-dimensions can be alternatively created inside the thin layer of low-band-gap semiconductor (AlGaAs-InGaAs-AlGaAs). Electrons of the 2DEG can be further confined, to create quantum dots, in the two-dimensional plane either by reducing the physical dimensions (vertical quantum dots) or by controlling electrons with top gates on the surface of the heterostructure (lateral quantum dots). Vertical quantum dots can be created by etching small pillars out of a larger semiconductor heterostructure. Electrons in a lateral gate-defined quantum-dot device

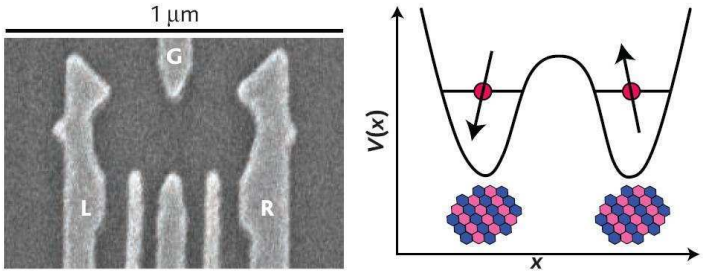


Figure 2.2: Scanning electron micrograph of a double quantum dot device and schematic representation of two electrons inside the device. (Adapted from Ref. [36] by Petta *et al.* ).

are confined by applying voltages on metallic top gates which deplete electrons underneath the gates [2, 3]. Examples of a lateral and a vertical quantum dot are shown in Fig. 2.1 and a lateral double quantum dot in Fig. 2.2.

There has been remarkable progress in controlling the few-electron single quantum dot devices during the last decade. However, some measurements require large arrays of (vertical) quantum dots to reach measurable signals. The number of electrons in the dot arrays is usually controlled by a single large back-gate. However, as there might be some variation in the sizes and shapes of individual quantum dots in the array also electron numbers may vary from dot to dot. This may lead to some undesired fluctuations in the experimental signals.

In this Thesis we consider the modeling of two-dimensional semiconductor quantum dots created in the two-dimensional electron gas where dot size is of the order of 100 nm. We model single quantum dot devices (or single quantum dot molecules), but corresponding experiments can be performed in single quantum dots or with quantum dot arrays. In GaAs 2DEG at low temperatures the electron mean-free path ($\sim 50\ \mu$m) is well above the quantum dot size and the Fermi wave length ($\sim$ 50 nm) is of the order of the device size [38]. Also phase-relaxation length can be much higher than device dimensions, enabling the observation of coherent quantum mechanical effects. This type of semiconductor quantum dots have energies in the range of meV's. Quantum mechanical properties are resolved only at low temperatures (T$<$ 4 K) and at low bias voltages excluding their direct use in commercial device applications. In this work we only consider closed, or isolated, quantum dots where electron wave functions are constricted inside quantum dot allowing transport experiments solely in the tunneling limit.

There is another type of semiconductor dots where the dot sizes are ultra-small, around 1 nm, and energies are in the range of eV's. These self-assembled quantum dots can be grown with molecular beam epitaxy when a lattice mismatched

strained semiconductor layer is grown on top of another semiconductor. After a critical thickness of the strained layer, atoms on the surface rearrange themselves spontaneously to release the stress and create small pyramids. The dot sizes can be made nearly equal with careful growth control but the arrangement of dots on the surface is pretty random. These self-assembled quantum dots bind both electrons and holes since the confinement is not created by gates (one can only apply either negative or positive voltage at a time), but by the small physical size of the dot. Therefore one can study inter-band optical properties of the dots [4, 39]. Exciton states in the self-assembled quantum dots can also be made lasing [40]. Even if these quantum dot lasers can operate at room temperatures (energies $\sim$ eV), the commercial applications are not directly achievable at present, due to the low output radiation power.

## 2.2 Experiments

In this section we briefly explain some experimental techniques relevant to the results presented in this Thesis. Many experiments on quantum dots have been concentrating on tunneling transport in the Coulomb blockade regime [41]. A small bias voltage $V_{sd}$ is applied between source and drain and the current is measured as a function of gate voltage $V_g$, see the left panel of Fig. 2.3. The gate voltage tunes the energy levels of a quantum dot, and as the energy reaches the Coulomb charging energy $e^2/2C$, an electron can enter the dot. ($C$ is the capacitance of the quantum dot). When an energy level is located inside the transport window, a current can pass through the dot. As the gate voltage is increased, the level moves out of the transport window and no electrons can tunnel inside or outside the dot, resulting in zero current. This is the Coulomb blockade region. The current is zero until another electron is drawn into the dot.

The energy required to add another electron is $E_{add} \approx e^2/C + \Delta\epsilon$ where also the energy separation of quantum mechanical energy levels $\Delta\epsilon$ must be taken into account. However, addition energies may depend strongly on the electron-electron interactions and such a simplified model may not be valid. White regions in the middle panel of Fig. 2.3 show zero current regions which are cut with narrow lines at the corners of the diamonds in the vertical axis. These show finite current through the dot.

If the source-drain voltage is tuned, transport is also allowed through the excited states of a certain charge state ($N$) and the $V_g$-$V_{sd}$ plot shows Coulomb diamonds where white color means zero current and other colors finite values of current. The evolution of the current peaks can also be traced as a function of magnetic field. The right panel of Fig. 2.3 shows the current peak as a function of gate voltage and magnetic field.

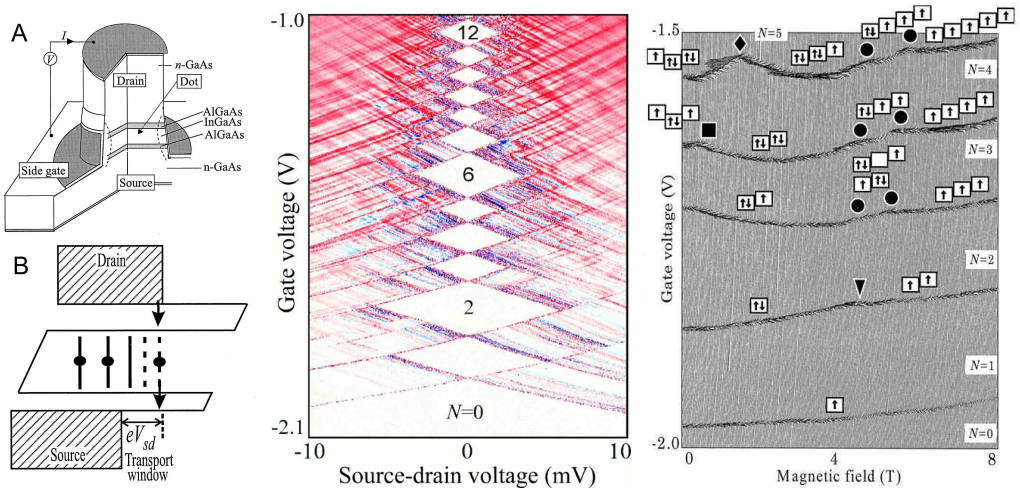


Figure 2.3: Left: Schematic of a vertical quantum dot (upper panel) and the transport through the dot (down). Middle: Differential conductance $\partial I/\partial V_{sd}$ as a function of gate voltage $V_g$ and bias voltage $V_{sd}$. In the white diamond-shaped regions $\partial I/\partial V_{sd} \approx 0$, as a result of Coulomb blockade. Right: Current $I$ as a function of magnetic field and gate voltage with the bias voltage of $V_{sd} = 0.1$ meV. (Adapted from Ref. [41] by Kouwenhoven *et al.* ).

Similar Coulomb blockade diagrams can be achieved with lateral quantum dots and lateral double quantum dots, although Coulomb diamonds, or honeycomb stability diagrams in the case of double dots, tend to be equal in size. This means that the energy shells, $\Delta\epsilon$, pay a lesser role in the addition energies [3, 13, 42]. This is a consequence of the large number of electrons in the lateral devices. Transport through a lateral double dot device has never been measured in the few-electron regime with one unpublished exception of a silicon double-dot device [26]. The problem is that the gates that are used to deplete the dots also strongly influence the tunnel barriers. Reducing electrons to the few-electron regime results in currents that are too small to be measured. Sensitive quantum point contact detectors placed nearby quantum dots allow, however, measurements in the few-electron regime [30, 33]. Another way to study addition energies and ground state evolution as a function of magnetic field in the few-electron regime is the single-electron capacitance spectroscopy (SECS) which is reviewed in Ref. [2].

The idea of far-infrared spectroscopy (FIR) is to use light of a suitable wavelength to induce excitations between energy levels in the quantum dot and measure the absorption spectrum of transmitted light through the sample. The evolution of the resonance peaks is studied as a function of the magnetic field. To get measurable signals, arrays of dots are needed. Typical FIR absorption peaks are

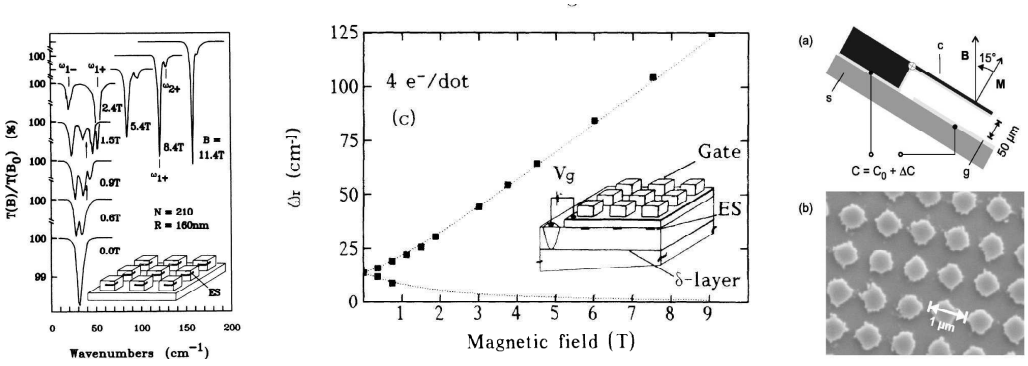


Figure 2.4: Left: Typical absorption peaks of far-infrared spectrum. (Adapted from Ref. [46] by Demel *et al.* ). Middle: Absorption peaks of far-infrared spectrum plotted as a function of magnetic field. (Adapted from Ref. [45] by Meurer *et al.* ). Right: Schematic of the magnetization measurement and scanning electron micrograph of a quantum dot array. (Adapted from Ref. [7] by Schwarz *et al.* ).

shown in the left panel of Fig. 2.4 and the energy of the absorbed light is plotted as a function of magnetic field in the middle panel.

However, FIR spectroscopy is rather insensitive for measuring interactions in the electron system and the observed transitions lie very close to the allowed excitation energies between single-particle states. FIR measurements tend to excite only the center-of-mass modes and thus the relative motion of electrons is not revealed. The reason is that for a circularly symmetric quantum dot confinement potentials, the center-of-mass and relative motions separate. FIR radiation couples only to the center-of-mass motion of the electrons in the dot [43]. Therefore the absorption peaks of FIR spectroscopy correspond to the excitation energies of the non-interacting system and are (almost) independent of the number of electrons in the dots [44, 45]. However, it soon became evident that also other features, not present in the center-of-mass motion of circular quantum dots, appear in the FIR spectra [46–49]. These require a non-circular confinement potential. How the electron-electron interactions and the shape of potential enter in the FIR absorption lines is highly non-trivial. The analysis of FIR spectra in quantum dot molecules is discussed in Publications **II**, **III** and **V** of this Thesis.

Magnetization measurements provide important information about the ground state properties of the low dimensional systems [50]. Unfortunately, the magnetic moment of an electron is tiny and the signals are too small to be measured directly on isolated quantum dots. However, the magnetizations of isolated quantum dots have been obtained indirectly by recalculating magnetizations from magneto-transport data [51]. Using highly sensitive micromechanical cantilevers,

magnetization of mesoscopic and nanoscale quantum dot arrays have been measured directly in recent experiments [7, 8]. Schematics of the measurement setup and the scanning electron micrograph of a quantum dot array is depicted in the right panel of Fig. 2.4.

# Chapter 3

# Theoretical basis

In quantum mechanics particles are described with wave functions $\Psi$ which are solutions of the non-relativistic Schrödinger equation:

$$\hat{\mathcal{H}}\Psi = i\hbar\frac{\partial\Psi}{\partial t}, \tag{3.1}$$

where $\hat{\mathcal{H}}$ is the Hamiltonian operator. In time-independent systems, as considered in this Thesis, the Schrödinger equation reduces to the energy eigenvalue problem

$$\hat{\mathcal{H}}\Psi = E\Psi. \tag{3.2}$$

All other physical properties can be calculated from the wave function $\Psi$. For all many-body quantum systems solving $\Psi$ becomes exponentially more difficult when the number of particles increases. With the aid of modern computing power, accurate solutions of $\Psi$ are achievable for few-particle quantum systems but for larger systems some approximative schemes of solving Eq. (3.2) are necessary.

## 3.1 Quantum dot Hamiltonian

As explained in Sec. 2.1, only a couple of electrons at time can be made free to move in the quantum dot region. The only constraint in the two-dimensional semiconductor interface is created by the external electrodes which define the shape and size of the quantum dot. Although an electron is effectively free to move, its motion is affected by the surrounding semiconductor material. One can rather accurately describe electron motion in a quantum dot by substituting the mass of a free electron with the effective mass of electrons of the host semiconductor material in the Hamiltonian ($m \to m^*$). This is called the effective-mass approximation and it has shown to be fairly accurate for GaAs conduction band

electrons in quantum dots. However, for electrons and holes in self-assembled quantum dots this may not be the case [4, 39]. We use effective mass approximation throughout this Thesis. We shall also exclude spin-orbit coupling from the quantum dot model Hamiltonian. This relativistic effect can become important in small quantum dots [4] but for large quantum dots it is negligible. It is worth to mention here, that spin-orbit interaction [28, 52, 53] along with fluctuating nuclear spins of GaAs lattice [31, 34, 36] can have a large effect on the decoherence times of spin states in large quantum dots, which are of great interest in the future spin-based information processing [20].

The model quantum dot Hamiltonian of $N$ electrons in a homogeneous external magnetic field along $z$ axis ($\mathbf{B} = B\mathbf{u}_z = \nabla \cdot \mathbf{A}$) can be written as

$$\begin{aligned} \hat{\mathcal{H}} &= \sum_i^N \left\{ \frac{\left(-i\hbar\nabla_i + \frac{e}{c}\mathbf{A}(\mathbf{r}_i)\right)^2}{2m^*} + V_{ext}(\mathbf{r}_i) + g^*\mu_B \mathbf{B}\cdot\hat{S}_i \right\} + \sum_{i<j}^N \frac{e^2}{\epsilon|\mathbf{r}_i - \mathbf{r}_j|} \\ &= \hat{\mathcal{H}}_0 + \hat{\mathcal{H}}_C. \end{aligned} \tag{3.3}$$

The first part in the parenthesis, $\hat{\mathcal{H}}_0$, shows the sum over N electrons in the quantum dot and the second interaction part, $\hat{\mathcal{H}}_C$, contains the Coulomb repulsion between electron pairs. Magnetic field appears in the Hamiltonian in the kinetic energy term via the vector potential ($\mathbf{A}(\mathbf{r}_i)$) and also couples directly to the electron spins ($\mathbf{B}\cdot\hat{S}_i = BS_{z,i}$). The potential $V_{ext}(\mathbf{r}_i)$ describes the quantum dot confinement of electrons. We assume electron motion in the quantum dot to be strictly restricted in two dimensions ($\mathbf{r} = x\mathbf{u}_x + y\mathbf{u}_y$). The semiconductor host of the quantum dot is taken into account also in effective g-factor $g^*$ and in dielectric constant $\epsilon$, in addition to effective mass of electrons $m^*$ discussed above.

## 3.2 Single-particle states

The direct solving of Schrödinger equation for the Hamiltonian of Eq. (3.3) is a tedious task and its discussion is postponed to next chapter. The Schrödinger equation for the single-particle part, $\hat{\mathcal{H}}_0$, on the other hand, is more straightforward to solve:

$$\hat{\mathcal{H}}_0\phi_i = \varepsilon_i\phi_i. \tag{3.4}$$

If we drop the interactions between electrons and the Zeeman coupling to the electron spin, the Hamiltonian for a single electron reduces to

$$\hat{\mathcal{H}}_0 = \frac{\left(-i\hbar\nabla_i + \frac{e}{c}\mathbf{A}(\mathbf{r}_i)\right)^2}{2m^*} + V_{ext}(\mathbf{r}_i). \tag{3.5}$$

### 3.2.1 Parabolic confinement

In many cases the confinement potential of a single quantum dot can be assumed to be parabolic:

$$V_{ext} = \frac{1}{2} m^* \omega_0^2 r^2, \tag{3.6}$$

where $\omega_0$ gives the strength of the confinement. In the case of large quantum dots (diameter $\sim 100$ nm) $\hbar\omega_0$ is typically of the order of a few meV.

Substituting harmonic $V_{ext}$ and $\mathbf{A}$ in the symmetric gauge ($\mathbf{A} = \frac{1}{2}B(-y, x, 0)$) we can rewrite Eq. (3.5) as

$$\hat{\mathcal{H}}_0 = -\frac{\hbar^2}{2m^*}\nabla^2 - i\hbar\frac{eB}{2m^*c}\left(-y\frac{\partial}{\partial x} + x\frac{\partial}{\partial y}\right) + \frac{e^2}{2m^*}\frac{B^2}{4c^2}r^2 + \frac{1}{2}m^*\omega_0^2 r^2, \tag{3.7}$$

which in a more compact form becomes

$$\hat{\mathcal{H}}_0 = -\frac{\hbar^2}{2m^*}\nabla^2 + \frac{1}{2}m^*\omega^2 r^2 + \frac{1}{2}\omega_c \hat{L}_z, \tag{3.8}$$

where $\omega^2 = \omega_0^2 + \omega_c^2/4$ and $\omega_c = eB/m^*c$. $\hat{L}_z$ is the $z$-component of the angular momentum operator ($\hat{L}_z = x\hat{p}_y - y\hat{p}_x = -i\hbar\partial/\partial\theta$).

A natural choice is to measure energy in oscillator units, $\hbar\omega$, and length in effective harmonic oscillator lengths, $l_\omega = \sqrt{\hbar/m^*\omega}$. The characteristic energy and length scales depend on the both confinement strength and magnetic field because $\omega = \sqrt{\omega_0^2 + \omega_c^2/4}$. The Hamiltonian in the oscillator units can be written as

$$\hat{\mathcal{H}}_0 = -\frac{1}{2}\nabla^2 + \frac{1}{2}r^2 + \frac{\omega_c}{2\omega}\hat{L}_z. \tag{3.9}$$

The problem of a harmonic oscillator in a magnetic field of Eq. (3.8) was first considered by Fock [54] and Darwin [55]. The solutions in polar coordinates can be written using the associated Laguerre polynomials $L_n^\alpha$(x):

$$\phi_{nl}(r,\theta) = \sqrt{\frac{n!}{\pi(n+|l|)!}}\; r^{|l|}\; L_n^{|l|}(r^2)\; e^{-r^2/2}\; e^{il\theta}, \tag{3.10}$$

where the Laguerre polynomials are given by the formula

$$L_n^{|l|}(x) = \sum_{m=0}^{n} \frac{(-1)^m}{m!}\binom{n+|l|}{n-m} x^m. \tag{3.11}$$

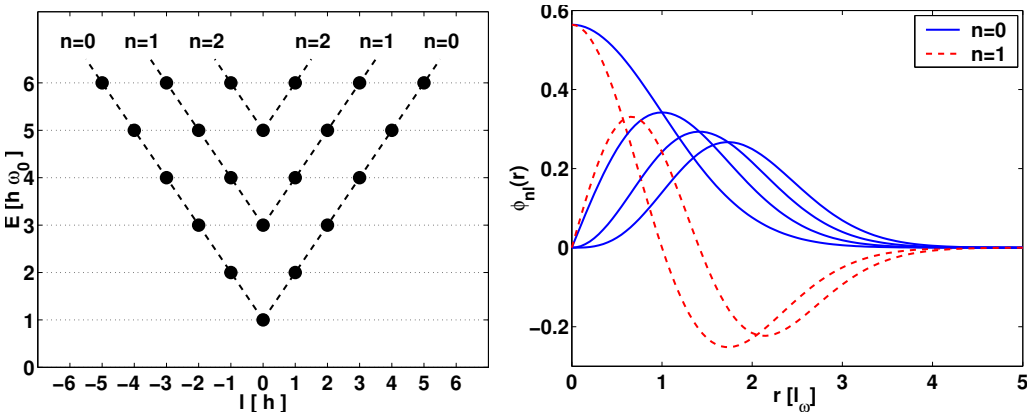


Figure 3.1: Left: Energy levels in the absence of magnetic field. Here $n$ denotes the radial quantum number and $l$ the angular quantum number. Right: Radial part of the wave functions $\phi_n(r)$ of Eq. (3.12).

The wavefunctions $\phi_{nl}$, called Fock-Darwin states, form a complete orthonormal basis. Ten lowest eigenstates of $\hat{\mathcal{H}}_0$ are

$$\begin{aligned}
\phi_{00} &= \frac{1}{\sqrt{\pi}} e^{-r^2/2} \\
\phi_{0\pm1} &= \frac{1}{\sqrt{\pi}}\, r\, e^{-r^2/2} e^{\pm i\theta} \\
\phi_{0\pm2} &= \frac{1}{\sqrt{\pi 2!}}\, r^2 e^{-r^2/2}\, e^{\pm 2i\theta} \\
\phi_{0\pm3} &= \frac{1}{\sqrt{\pi 3!}}\, r^3 e^{-r^2/2}\, e^{\pm 3i\theta} \\
\phi_{10} &= \frac{1}{\sqrt{\pi}}\, (1-r^2)\, e^{-r^2/2} \\
\phi_{1\pm1} &= \frac{1}{\sqrt{\pi 2!}}\, r(2-r^2)\, e^{-r^2/2}\, e^{\pm i\theta}.
\end{aligned} \tag{3.12}$$

The corresponding energy eigenvalues of the radial quantum number $n$ and the angular quantum number $l$ of $\hat{\mathcal{H}}_0$ are given by

$$\varepsilon_{nl} = (2n + 1 + |l|)\hbar\omega - \frac{1}{2} l \hbar\omega_c. \tag{3.13}$$

In the absence of the magnetic field, the solution reduces to a two-dimensional harmonic oscillator. When $B = 0$ the last term of Eq. (3.13) vanishes ($\omega_c = 0$) and all combinations of $(2n + |l|) =$ constant are degenerate in energy. The

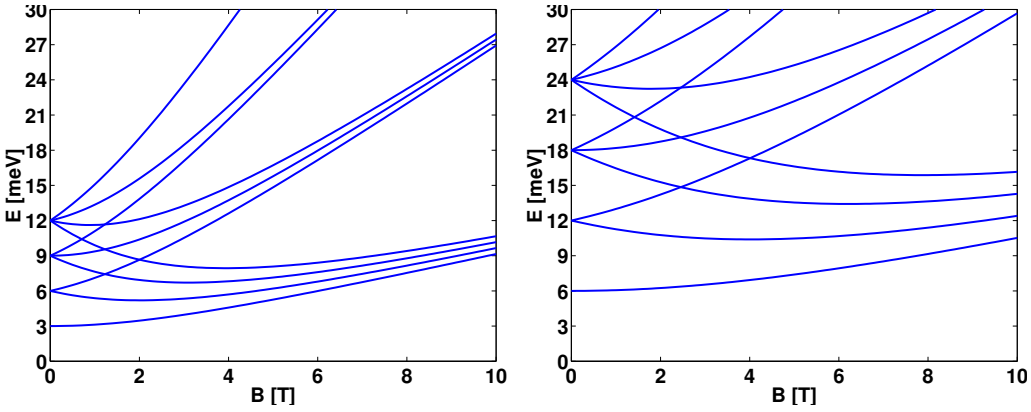


Figure 3.2: Fock-Darwin energy levels as a function of magnetic field with external confinement of $\hbar\omega_0 = 3$ meV in the left and $\hbar\omega_0 = 6$ meV in the right panel.

degeneracy becomes larger with higher energies. The energy levels $\varepsilon_{nl}$ at $B = 0$ T are plotted in the left panel of Fig. 3.1 and the radial parts of wave functions of Eq. (3.12) are plotted in the right panel of Fig. 3.1.

Application of a magnetic field destroys the degeneracy due to the term linear in $l$. The electron levels shift and split, resulting in many level crossings as the magnetic field strength increases. In the left panel of Fig. 3.2 the evolution of the five lowest energy levels $(n, l)$ is plotted as a function of magnetic field with the confinement strength $\hbar\omega_0 = 3$ meV. For a comparison, the single-particle energy levels of $\hbar\omega_0 = 6$ meV parabolic quantum dot are plotted in the right panel of Fig. 3.2. When we are in the limit of a very high magnetic field the lowest energy levels condense into Landau levels. The lowest Landau level is composed of increasing $l$-values with $n = 0$, whose energy rises with increasing $B$, but the separation between the energy levels decreases when the magnetic field increases. In the limit of $B \to \infty$ the degeneracy in the lowest Landau level becomes very high.

### 3.2.2 Quantum-dot molecules

We model quantum-dot molecules (QDMs) with parabolic minima separated by a finite distance. Then the the confinement potential $V_{ext}$ can be written as

$$V_{ext}(\mathbf{r}) = \frac{1}{2} m^* \omega_0^2 \min \left\{ \sum_j^M (\mathbf{r} - \mathbf{L}_j)^2 \right\}, \tag{3.14}$$

where $\mathbf{L}_j$'s ($\mathbf{L}_j = (L_x, L_y)$) give the positions of the minima of QDM potential and $M$ is the number of minima. When $\mathbf{L}_1 = (0, 0)$ (and $M = 1$) we have a

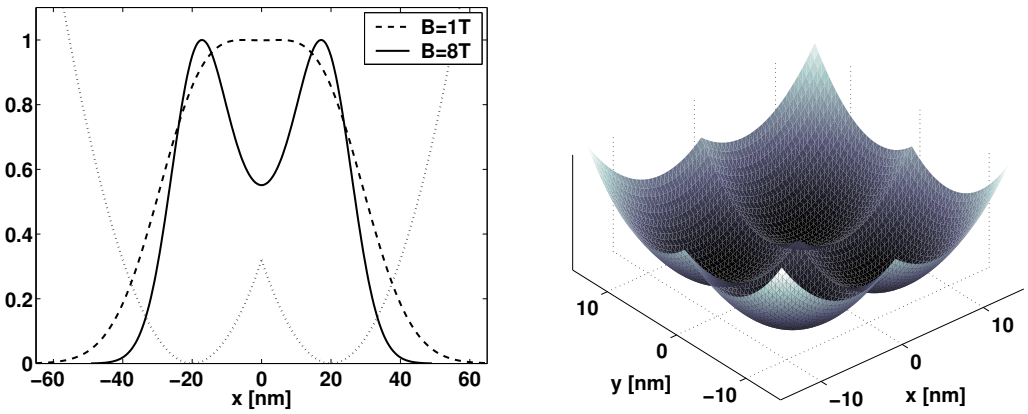


Figure 3.3: Left: Confinement potential $V_{ext}$ of $L_x = 20$ nm double dot (dotted line) and ground state single-particle density $|\phi_0|^2$ along $y = 0$ at $B = 1$ and 8 T. The maximum value of $|\phi_0|^2$ is scaled to unity. Right: Confinement potential of $L_x = L_y = 5$ nm four-minima quantum-dot molecule.

single parabolic quantum dot. With $M = 2$ and $\mathbf{L}_{1,2} = (\pm L_x, 0)$ we get a double-dot potential. We also study four-minima QDM ($M = 4$) with the minima at four possibilities of $(\pm L_x, \pm L_y)$. We study both square-symmetric ($L_x = L_y$) and rectangular-symmetric ($L_x \neq L_y$) four-minima QDMs. The confinement potential can also be written using the absolute values of $x$ and $y$ coordinates as

$$\begin{aligned} V_{ext}(x,y) &= \frac{1}{2}m^*\omega_0^2 \times \\ &\quad \left[r^2 - 2L_x|x| - 2L_y|y| + L_x^2 + L_y^2\right] \ . \end{aligned} \tag{3.15}$$

For non-zero $L_x$ and $L_y$, the perturbation to the parabolic potential comes from the linear terms of $L_x$ or $L_y$ that contain also the absolute value of the associated coordinate. We mainly use $\hbar\omega_0 = 3$ meV in this Thesis.

For this type of quantum dot molecules, no analytic solutions are available, but with numerical methods one can solve single-particle energies and wave functions:

$$\hat{\mathcal{H}}_0\phi_i = \varepsilon_i\phi_i. \tag{3.16}$$

The left panel of Fig. 3.3 shows ground state single-particle density $|\phi_0|^2$ of a two-dimensional ($L_x = 20$ nm, $L_y = 0$) double dot along $x$ axis at $B = 1$ and 8 T. The double dot potential profile is plotted with a dotted line. In $y$ direction the double dot $V_{ext}$ is still parabolic. With large $L_x$ and strong $B$ the single-particle density starts to localize near the minima. We use nanometers (nm) and meV's instead of oscillator units with quantum-dot molecules. The right panel of

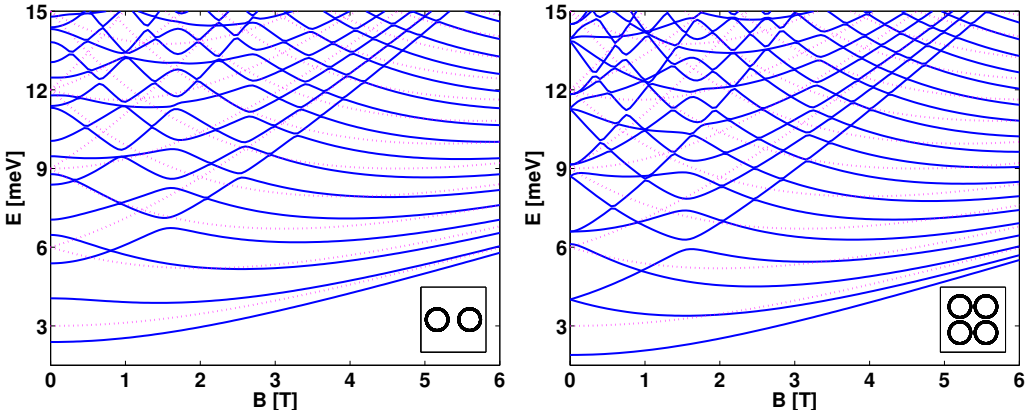


Figure 3.4: Energy levels as a function of magnetic field of $\hbar\omega_0 = 3$ meV, $L_x = 15$ double dot in the left panel and $L_x = L_y = 10$ nm four-minima quantum-dot molecule in the right panel. Dotted lines show Fock-Darwin energy levels of $\hbar\omega_0 = 3$ meV parabolic quantum dot.

Fig. 3.3 shows the confinement potential $V_{ext}$ of square-symmetric four-minima quantum-dot molecule.

The energy levels as a function of magnetic field of a double dot and a four-minima quantum-dot molecule are shown in Fig. 3.4. The dotted lines show Fock-Darwin energy levels of $\hbar\omega_0 = 3$ meV parabolic quantum dot. Compared to parabolic confinement, in quantum-dot molecules many levels shift and split and there are gaps or avoided crossings with some energy levels.

## 3.3 Many-electron states

In the quantum realm of many identical particles, some extra conditions have to be considered when solving the Schrödinger equation (3.2). The many-body wave function, that describes $N$ quantum-mechanical particles each having space and spin coordinates $(\mathbf{r}_i, \xi_i)$,

$$\Psi = \Psi\left[(\mathbf{r}_1, \xi_1), (\mathbf{r}_2, \xi_2), ..., (\mathbf{r}_N, \xi_N)\right] \tag{3.17}$$

must obey certain rules before it can describe the real quantum world. First of all, similar particles are indistinguishable in the quantum theory. Therefore we cannot state, for example, which of the electron is observed in an experiment, but we can only say that one of them was observed. Identical particles cannot be labeled in quantum mechanics. Secondly, electrons are fermions which have half-integer intrinsic angular moment, spin, that can have the quantum number

$s_z = \pm\frac{1}{2}\hbar$. Fermions obey Fermi statistics and according to the Pauli exclusion principle, no electrons with the same spin can occupy a same quantum state. Indistinguishability and Fermi statistics set a requirement for an antisymmetric many-electron total wave function. The antisymmetric wave function ensures that if two fermions of same spin have equal coordinates the wave function automatically results zero. In the next two subsections we show in more detail how to include spin wave functions $\chi_i(\xi)$ and construct antisymmetric many-electron wave functions.

### 3.3.1 Spin

We introduce the spin coordinate $\xi$ that can take two values $\pm 1$ and spin wave functions $\chi_\uparrow$ and $\chi_\downarrow$ as

$$\begin{aligned}\chi_\uparrow(\xi) &= \begin{cases} 1, & \text{if } \xi = 1 \\ 0, & \text{if } \xi = -1 \end{cases} \\ \chi_\downarrow(\xi) &= \begin{cases} 0, & \text{if } \xi = 1 \\ 1, & \text{if } \xi = -1 \end{cases}\end{aligned} \tag{3.18}$$

If there are no terms mixing space and spin coordinates in the Hamiltonian, we can rewrite the single-particle wave function as

$$\psi_i(x) = \phi_i(\mathbf{r})\chi_i(\xi), \tag{3.19}$$

where $x$ denotes both $\mathbf{r}$ and $\xi$. Integration over $x$ means normal integration over the space coordinate $\mathbf{r}$ and summation over the spin coordinate $\xi$:

$$\int \psi_i^*(x)\psi_i(x)dx = \sum_{\xi=\pm 1} \int \phi_i^*(\mathbf{r})\phi_i(\mathbf{r})\chi_i(\xi)\chi_i(\xi). \tag{3.20}$$

If the spatial wave functions are normalized we have

$$\int |\psi_i(x)|^2 = \int |\phi(\mathbf{r})|^2 d\mathbf{r} \sum_{\xi=\pm 1} \chi_i^2(\xi) = 1. \tag{3.21}$$

### 3.3.2 Antisymmetric wave functions

Supposing we have a set of single-particle levels from 1 to $N$ $\{\psi_{c_i}\}_{i=1}^N$, where $c_i$ denotes both space and spin quantum numbers, and we want to construct an antisymmetric many-body wave function for $N$ electrons. We are considering quantum particles which are indistinguishable. Clearly it should not be possible to say which particle is in which state $c_i$. We can only state that we have a

collection of particles that occupy levels $\{c_i\}_{i=1}^{N}$. Therefore, the simple product of single-particle wave functions is not correct. Also, we are considering fermions. A single-particle level cannot be occupied by two particles having exactly same quantum numbers (the single-particle level index and spin). This requirement is satisfied if we make an antisymmetric wave function, which changes sign when any two coordinates are exchanged. The antisymmetric wave function can be constructed by starting from the product $\psi_{c_1}(x_1)\psi_{c_2}(x_2)\dots\psi_{c_N}(x_N)$ and permuting the coordinates $x_i$ in every possible way. There are $N!$ ways to do this. The sign of the product is changed every time two coordinates are exchanged. The antisymmetric wave function is obtained when all possible permutations with the signs are summed up:

$$\Phi(x_1,\dots,x_N) = \frac{1}{(N!)^{1/2}}\sum_P (-1)^P P\psi_{c_1}(x_1)\psi_{c_2}(x_2)\dots\psi_{c_N}(x_N). \tag{3.22}$$

The permutation can be written in compact form as a Slater determinant:

$$\Phi(x_1,\dots,x_N) = \frac{1}{(N!)^{1/2}}\begin{vmatrix} \psi_{c_1}(x_1) & \psi_{c_1}(x_2) & \dots & \psi_{c_1}(x_N) \\ \psi_{c_2}(x_1) & \psi_{c_2}(x_2) & \dots & \psi_{c_2}(x_N) \\ \vdots & \vdots & & \vdots \\ \psi_{c_N}(x_1) & \psi_{c_N}(x_2) & \dots & \psi_{c_N}(x_N) \end{vmatrix}. \tag{3.23}$$

We can see that the Pauli exclusion principle is satisfied since if any two $c_i$'s are same the two lines in the determinant are identical. Identical lines in a determinant result always zero and therefore the wave function vanishes automatically.

The wave function $\Phi(x_1,\dots,x_N)$ obeys the rules of many-electron quantum mechanics and therefore all wave functions of *electrons* that are solutions of the Scrödinger equation must be antisymmetric. However, solving the Shrödinger equation of a Hamiltonian for more than one electron is very difficult. Analytical solutions are available for two interacting electrons in some special cases [56] and numerical solutions are also possible for a very limited number of electrons. Usually, not more than ten electrons can be described accurately. We will consider solving the few-particle Shrödinger equation in the next chapter.

# Chapter 4

# Diagonalization of Hamiltonian matrix

## 4.1 Matrix formulation of quantum mechanics

Suppose we have a complete set of orthonormal functions $\phi_n(x)$ and we are interested in solving a (single-particle) Schrödinger equation $\hat{H}\psi(x) = E\psi(x)$. We can expand any function of $x$ in terms of a complete orthonormal set $\phi_n(x)$:

$$\psi(x) = \sum_{n=0}^{\infty} a_n \phi_n(x). \tag{4.1}$$

$\psi(x)$ can be equivalently be determined with the coefficients $a_n$ of the expansion:

$$\psi(x) \iff \{a_n\} \iff \begin{pmatrix} a_1 \\ a_2 \\ a_3 \\ \vdots \end{pmatrix}. \tag{4.2}$$

For a proper normalization we demand $\sum_{n=0}^{\infty} |a_n|^2 = 1$. Now, the Schrödinger equation $\hat{H}\psi = E\psi$ can be written with the set $\phi_n(x)$:

$$\hat{H}\left(\sum_n a_n \phi_n(x)\right) = E\left(\sum_n a_n \phi_n(x)\right). \tag{4.3}$$

Multiplying Eq. (4.3) on the left by $\phi_m^*(x)$ and integrating over the space we get

$$\begin{aligned} \int \phi_m^*(x)\ \hat{H}\left(\sum_n a_n \phi_n(x)\right) dx &= \int \phi_m^*(x) E\left(\sum_n a_n \phi_n(x)\right) dx \\ \sum_n a_n \langle \phi_m | \hat{H} | \phi_n \rangle &= E \sum_n a_n \underbrace{\langle \phi_m | \phi_n \rangle}_{\delta_{n,m}}. \end{aligned} \tag{4.4}$$

We assume a shorthand notation for the matrix element

$$\langle \phi_m | \hat{H} | \phi_n \rangle = H_{nm} \tag{4.5}$$

and now we can write the Schrödinger equation in a matrix form:

$$\begin{pmatrix} H_{11} & H_{12} & H_{13} & \dots \\ H_{21} & H_{22} & H_{23} & \dots \\ H_{31} & H_{32} & H_{33} & \dots \\ \vdots & \vdots & \vdots & \ddots \end{pmatrix} \begin{pmatrix} a_1 \\ a_2 \\ a_3 \\ \vdots \end{pmatrix} = E \begin{pmatrix} a_1 \\ a_2 \\ a_3 \\ \vdots \end{pmatrix}. \tag{4.6}$$

We have thus formulated our original problem of finding the eigenvalues and vectors of the Hamiltonian $\hat{H}\psi = E\psi$ in the matrix presentation. The solution of the Schrödinger equation is equivalent of finding the eigenvalues and eigenvectors of the matrix. If we had chosen the basis $\psi_n$ to be the solutions of the single-particle Hamiltonian $\hat{H}\phi_n = E_n\phi_n$ and used those states in the expansion, we would have

$$H_{nm} = \langle \phi_m | \hat{H} | \phi_n \rangle = \langle \phi_m | E_n | \phi_n \rangle = E_n \delta_{nm}. \tag{4.7}$$

Then our matrix is already diagonal and energy eigenvalues can be read immediately from the diagonal of the matrix:

$$\begin{pmatrix} E_1 & 0 & 0 & \dots \\ 0 & E_2 & 0 & \dots \\ 0 & 0 & E_3 & \dots \\ \vdots & \vdots & \vdots & \ddots \end{pmatrix} \begin{pmatrix} a_1 \\ a_2 \\ a_3 \\ \vdots \end{pmatrix} = E \begin{pmatrix} a_1 \\ a_2 \\ a_3 \\ \vdots \end{pmatrix}. \tag{4.8}$$

The matrix equation (4.8) can be satisfied only if

$$det(\mathbf{H} - E\mathbf{I}) = det \begin{vmatrix} E_1 - E & 0 & 0 & \dots \\ 0 & E_2 - E & 0 & \dots \\ 0 & 0 & E_3 - E & \dots \\ \vdots & \vdots & \vdots & \ddots \end{vmatrix} = 0. \tag{4.9}$$

If we do not know the solution of the Schrödinger equation, we can express the Hamiltonian in the matrix formulation with any complete basis we wish to choose and the eigenvalues and vectors can be found by diagonalizing the Hamiltonian. However, the matrix is infinite dimensional, whereas in real calculations we include only some finite number of states in the expansion and then diagonalize the matrix in a truncated basis. The convergence can be checked by adding more states $\phi_n$ in the expansion and studying the change in the eigenvalues as the basis size and the matrix dimensions are increased.

In the case of interacting electrons, we can expand the many-electron wave function using a set of basis functions. According to quantum theory, these basis functions must be antisymmetric. The problem can be formulated in the matrix form also in the interacting few-particle system. Supposing we have a complete set of $N$-particle wave functions $\Phi_{\mathbf{c}}$ (the set of determinants with all possible combinations of different single-particle states $c_i$), we can search the solution for the interacting few-particle Hamiltonian

$$\hat{\mathcal{H}}\Psi = (\hat{\mathcal{H}}_0 + \hat{\mathcal{H}}_C)\Psi = E\Psi \tag{4.10}$$

by expanding the wave function $\Psi$ in this basis:

$$\Psi = \sum_{\mathbf{c}} A_{\mathbf{c}}\Phi_{\mathbf{c}}, \tag{4.11}$$

where the summation runs over all possible determinantal wave functions (where determinantal refers to the antisymmetric many-body wave functions, Eq. (3.23)). The Schrödinger equation reads

$$\hat{\mathcal{H}}\left(\sum_{\mathbf{c}} A_{\mathbf{c}}\Phi_{\mathbf{c}}\right) = E\left(\sum_{\mathbf{c}} A_{\mathbf{c}}\Phi_{\mathbf{c}}\right). \tag{4.12}$$

If we multiply Eq. (4.12) by $\Phi^*_{\mathbf{d}}$ on left and integrate over all variables $x_i$, we can write the Hamiltonian in the matrix form with the matrix elements as

$$H_{\mathbf{dc}} = \langle\Phi_{\mathbf{d}}|\hat{\mathcal{H}}|\Phi_{\mathbf{c}}\rangle. \tag{4.13}$$

The matrix elements can be calculated and by diagonalizing the matrix we obtain the eigenvalues and eigenvectors of the Hamiltonian. When calculating the matrix elements, the $\Phi_{\mathbf{c}}$'s are now the antisymmetric wave functions of the $N$-electron system and $\hat{\mathcal{H}}$ is the interacting Hamiltonian. However, as in the single-particle case, the matrix is infinite dimensional, but again, by truncating the matrix we can solve the eigenvalues and the convergence can be checked by increasing the number of basis states. The matrix is usually diagonalized numerically. In principle the approach seems ideal for solving interacting few-body systems, but in practice only very small number of particles can be calculated with good accuracy ($\mathrm{N} \lesssim 10$).

## 4.2 Matrix elements for quantum-dot molecules

In this Thesis we consider mainly two quantum mechanical electrons in quantum-dot molecules. The Hamiltonian for the two interacting electrons can be written

as

$$\hat{\mathcal{H}} = \sum_i^2 \left\{ \frac{\left(-i\hbar\nabla_i + \frac{e}{c}\mathbf{A}(\mathbf{r}_i)\right)^2}{2m^*} + V_{ext}(\mathbf{r}_i) + g^*\mu_B B s_{z,i} \right\} + \frac{e^2}{\epsilon r_{12}}. \tag{4.14}$$

Substituting the quantum-dot molecule confinement potential of Eq. (3.15) in the Hamiltonian and switching to oscillator units ($E = \hbar\omega, l_\omega = \sqrt{\hbar/m^*\omega}$), we can rewrite the Hamiltonian as

$$\begin{aligned} \hat{\mathcal{H}} &= \sum_i^2 \left\{ -\frac{1}{2}\nabla_i^2 + \frac{1}{2}r_i^2 + i\frac{\omega_c}{2\omega}\left(-y_i\frac{\partial}{\partial x_i} + x_i\frac{\partial}{\partial y_i}\right) \right. \\ &\quad \left. + \frac{\omega_0^2}{2\omega^2}\left(L_x^2 + L_y^2 - 2L_x|x_i| - 2L_y|y_i|\right) + \gamma^*\hat{S}_{z,i} \right\} + \frac{C}{r_{12}} \\ &= \sum_i^2 \hat{\mathcal{H}}_{0,i} + \hat{\mathcal{H}}_C, \end{aligned} \tag{4.15}$$

where $\omega^2 = \omega_0^2 + \omega_c^2/4$, $\omega_c = eB/m^*c$ and $\gamma^* = g^*\mu_B B/\hbar\omega$ . Here $C$ is the Coulomb strength $C = \sqrt{\frac{Ha}{\hbar\omega}}\frac{\sqrt{m^*/m_e}}{\epsilon}$, where $Ha$ is Hartree $\approx 27.2$ eV.

The spin-dependent part of the Hamiltonian is not very complicated and the four possible spin eigenstates of $\hat{S}^2$ and $\hat{S}_z$ are rather straightforward to obtain [57]. For the anti-symmetric spin singlet ($S = 0$) we have solution

$$|S\rangle = \tfrac{1}{\sqrt{2}}\left(\chi_\uparrow(\xi_1)\chi_\downarrow(\xi_2) - \chi_\uparrow(\xi_2)\chi_\downarrow(\xi_1)\right), \quad S = S_z = 0, \tag{4.16}$$

and for the symmetric spin triplet ($S = 1$) we have three possible eigenstates

$$\begin{aligned} |T_+\rangle &= \chi_\uparrow(\xi_1)\chi_\uparrow(\xi_2), && S = 1, S_z = 1, \\ |T_0\rangle &= \tfrac{1}{\sqrt{2}}\left(\chi_\uparrow(\xi_1)\chi_\downarrow(\xi_2) + \chi_\uparrow(\xi_2)\chi_\downarrow(\xi_1)\right), && S = 1, S_z = 0, \\ |T_-\rangle &= \chi_\downarrow(\xi_1)\chi_\downarrow(\xi_2), && S = 1, S_z = -1. \end{aligned} \tag{4.17}$$

As there is no coupling between the spin and space coordinates in the Hamiltonian, we shall write the two-electron wave function as a product of space and spin wave functions ($\Psi = \Psi_S(\mathbf{r}_1, \mathbf{r}_2)\chi_S(\xi_1, \xi_2)$). Actually, as we already know the spin eigenstates, it is sufficient to expand the spatial part in symmetric functions for the spin singlet ($S = 0$) and antisymmetric functions for the spin triplet ($S = 1$). Total wave function must be antisymmetric. The space part of the wave function is

$$\Psi_S(\mathbf{r}_1, \mathbf{r}_2) = \sum_{i\le j} \alpha_{i,j}\{\phi_i(\mathbf{r}_1)\phi_j(\mathbf{r}_2) + (-1)^S\phi_i(\mathbf{r}_2)\phi_j(\mathbf{r}_1)\}, \tag{4.18}$$

where $\alpha_{i,j}$'s are complex coefficients and $\phi$'s are single-particle states. For these we choose the two-dimensional Gaussians

$$\phi_i(\mathbf{r}) = \phi_{n_{x,i},n_{y,i}}(x,y) = x^{n_{x,i}} y^{n_{y,i}} e^{-r^2/2}, \tag{4.19}$$

where $n_{x,i}$ and $n_{y,i}$ are integers and $i$ is a shorthand notation for the pair $(n_{x,i}, n_{y,i})$. For this choice, neither the single-particle functions nor the two-body functions are orthogonal. Therefore, when constructing the matrix to be diagonalized we need to calculate also matrix elements of overlap integrals $S_{i,j} = \int \phi_i \phi_j$. The diagonalization of the Hamiltonian matrix is now a generalized eigenvalue problem

$$H\alpha = ES\alpha, \tag{4.20}$$

where $H$ is the Hamiltonian matrix, $\alpha$ is the vector of complex coefficients $\alpha_{i,j}$, $S$ is the overlap matrix and $E$ is the energy eigenvalue. The reason for this choice of $\phi_i$ is that the matrix elements are rather stable and easy to calculate. By diagonalizing the matrix we get all energy eigenvalues and all eigenvectors.

We need to calculate all matrix elements of the Hamiltonian and overlap integrals. For the single-particle part $\mathcal{H}_0$, excluding the Zeeman term, the integrals are of type

$$H^0_{ijkl} = \int \phi_i \mathcal{H}_0 \phi_k \int \phi_j \phi_l. \tag{4.21}$$

The integration is over two-dimensional space ($\int_{-\infty}^{\infty} dxdy$) and $i$ denotes the pair $(n_{x,i}, n_{y,i})$ and similarly for the quantum numbers $j, k$, and $l$. For the Coulomb interaction part, we need to calculate terms of the following type

$$H^C_{ijkl} = \int d\mathbf{r}_1 d\mathbf{r}_2 \phi_i(\mathbf{r}_1)\phi_k(\mathbf{r}_2)\frac{1}{r_{12}}\phi_j(\mathbf{r}_2)\phi_l(\mathbf{r}_1). \tag{4.22}$$

We start our calculation of the matrix elements by the definition of the gamma function

$$\Gamma(z) = 2\int_0^{\infty} e^{-t^2} t^{2z-1} dt, \tag{4.23}$$

where $z$ is real in our case. We will first consider the overlap integral $S_{i,j} = \int \phi_i \phi_j$, which can be separated to two one-dimensional integrals which in the end results simple gamma function integrals. If $n_{x,i} + n_{n,j}$ or $n_{y,i} + n_{y,j}$ is odd, $S_{i,j} = 0$. Otherwise $S_{i,j} = \Gamma[1/2 + (n_{x,i} + n_{x,j})/2]\Gamma[1/2 + (n_{y,i} + n_{y,j})/2]$. For all even and odd values of $n_{x,i} + n_{n,j}$ and $n_{y,i} + n_{y,j}$ this can be written as

$$\begin{aligned} \int \phi_i \phi_j &= \frac{1}{2}\left[1 + (-1)^{n_{x,i}+n_{x,j}}\right] \times \frac{1}{2}\left[1 + (-1)^{n_{y,i}+n_{y,j}}\right] \\ &\times \Gamma\left[\frac{1}{2} + \frac{1}{2}(n_{x,i} + n_{x,j})\right] \times \Gamma\left[\frac{1}{2} + \frac{1}{2}(n_{y,i} + n_{y,j})\right] \end{aligned} \tag{4.24}$$

For the calculation of $H_0^{ij} = \int \phi_i \mathcal{H}_0 \phi_j$ we first write it as

$$H_{ij}^0 = \int \phi_i \frac{\mathcal{H}_0 \phi_j}{\phi_j} \phi_j, \tag{4.25}$$

which replaces the operator $\mathcal{H}_0$ with a function (called local energy in quantum Monte Carlo)

$$\begin{aligned} \frac{\mathcal{H}_0 \phi_j}{\phi_j} &= 1 + n_x + n_y + \frac{n_x(n_x-1)}{2x^2} + \frac{n_y(n_y-1)}{2y^2} + i\frac{\omega_c}{2\omega}\left(n_y \frac{x}{y} - n_x \frac{y}{x}\right) \\ &+ \frac{\omega_0^2}{2\omega^2}\left(L_x^2 + L_y^2 - 2L_x|x_i| - 2L_y|y_i|\right). \end{aligned} \tag{4.26}$$

Besides the overlap integral, we need three other types of integrals:

$$\begin{aligned} \int \phi_i \frac{1}{x^2} \phi_j &= \frac{1}{2}\left[1 + (-1)^{n_{x,i}+n_{x,j}}\right] \times \frac{1}{2}\left[1 + (-1)^{n_{y,i}+n_{y,j}}\right] \\ &\times \Gamma\left[\frac{1}{2}(-1 + n_{x,i} + n_{x,j})\right] \times \Gamma\left[\frac{1}{2}(1 + n_{y,i} + n_{y,j})\right], \end{aligned} \tag{4.27}$$

$$\begin{aligned} \int \phi_i \frac{y}{x} \phi_j &= \frac{1}{2}\left[-1 + (-1)^{n_{x,i}+n_{x,j}}\right] \times \frac{1}{2}\left[-1 + (-1)^{n_{y,i}+n_{y,j}}\right] \\ &\times \Gamma\left[\frac{1}{2}(n_{x,i} + n_{x,j})\right] \times \Gamma\left[\frac{1}{2}(2 + n_{y,i} + n_{y,j})\right], \end{aligned} \tag{4.28}$$

and

$$\begin{aligned} \int \phi_i |x| \phi_j &= \frac{1}{2}\left[1 + (-1)^{n_{x,i}+n_{x,j}}\right] \times \frac{1}{2}\left[1 + (-1)^{n_{y,i}+n_{y,j}}\right] \\ &\times \Gamma\left[\frac{1}{2}(2 + n_{x,i} + n_{x,j})\right] \times \Gamma\left[\frac{1}{2}(1 + n_{y,i} + n_{y,j})\right]. \end{aligned} \tag{4.29}$$

In all these formulas the first rows are delta functions depending on the parity of the sums of $n_x$'s and $n_y$'s.

The interaction term

$$H_{ijkl}^C = \int d\mathbf{r}_1 \; d\mathbf{r}_2 \; \phi_i(\mathbf{r}_1)\phi_j(\mathbf{r}_2)\frac{1}{r_{12}}\phi_k(\mathbf{r}_2)\phi_l(\mathbf{r}_1) \tag{4.30}$$

can also be calculated analytically. We start by Fourier transforming the $1/r_{12}$ term:

$$\frac{1}{r_{12}} = \frac{1}{2\pi}\int d\mathbf{k} \; \frac{1}{k} e^{i\mathbf{k}\cdot\mathbf{r}_{12}}, \tag{4.31}$$

and arranging terms gives

$$H^C_{ijkl} = \frac{1}{2\pi}\int d\mathbf{k}\; d\mathbf{r}_1\; d\mathbf{r}_2\; \frac{1}{k} \quad x_1^{n_1} e^{-x_1^2+ik_x x_1}\; y_1^{n_2} e^{-y_1^2+ik_y y_1} \\ \times \quad x_2^{n_3} e^{-x_2^2-ik_x x_2}\; y_2^{n_4} e^{-y_2^2-ik_y y_2} \quad , \tag{4.32}$$

where $\mathbf{k}$ is also two-dimensional and $n_1 = n_{x,i} + n_{x,j}$, and so on. Next we substitute

$$x^n e^{-x^2+ikx} = \lim_{a\to 0} \frac{\partial^n}{\partial a^n} e^{-x^2+ikx+ax}, \tag{4.33}$$

and we can integrate over each Cartesian coordinate as

$$\int dx \frac{\partial^n}{\partial a^n} e^{-x^2+ikx+ax} = \frac{\partial^n}{\partial a^n}\int dx e^{-x^2+ikx+ax} = \frac{\partial^n}{\partial a^n}\sqrt{\pi} e^{(ik+a)^2/4}. \tag{4.34}$$

The resulting derivative can be calculated as

$$\begin{aligned} \frac{\partial^n}{\partial a^n} e^{(ik+a)^2/4}|_{a=0} &= i^n \frac{\partial^n}{\partial k^n} e^{(ik+a)^2/4}|_{a=0} = \left(\frac{i}{2}\right)^n \frac{\partial^n}{\partial(\frac{k}{2})^n} e^{-(k/2)^2} \\ &= \left(-\frac{i}{2}\right)^n e^{-(k/2)^2} H_n(k/2), \end{aligned} \tag{4.35}$$

where $H_n$ is a Hermite polynomial. Performing this procedure to all terms of $V_{ijkl}$ results

$$\begin{aligned} H^C_{ijkl} &= \frac{\pi}{2}\int k dk d\theta \left(-\frac{i}{2}\right)^{\sum n_i} e^{-(k/2)^2} H_{n_1}\left(\frac{kcos\theta}{2}\right) H_{n_2}\left(\frac{ksin\theta}{2}\right) \\ &\times H_{n_3}\left(\frac{-kcos\theta}{2}\right) H_{n_4}\left(\frac{-ksin\theta}{2}\right), \end{aligned} \tag{4.36}$$

where the $\mathbf{k}$-integral is written in the cylindrical coordinates. This integral can be calculated by writing each $H_n$ in series form, and each term in this series can be written as a constant times a product of integrals of the type

$$\int dk e^{-k^2/2} k^{nn+mm} = 2^{(nn+mm-1)/2}\Gamma\left[\frac{1}{2}(nn+mm+1)\right] \tag{4.37}$$

and

$$\int d\theta cos^{nn}(\theta) sin^{mm}(\theta) = 2\frac{\Gamma\left[\frac{1}{2}(nn+1)\right]\Gamma\left[\frac{1}{2}(mm+1)\right]}{\Gamma\left[\frac{1}{2}(nn+mm+1)\right]} \tag{4.38}$$

for both $nn$ and $mm$ even and zero otherwise. The final $V_{ijkl}$ is a multiple sum over many terms where each of them contains several gamma functions.

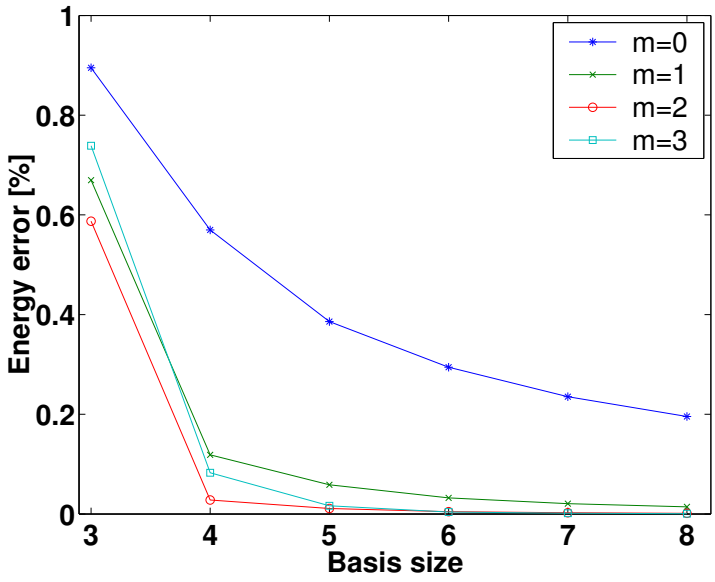


Figure 4.1: Relative error in the energy of parabolic two-electron quantum dot at $B = 0$ as a function of the basis size $n = n_x = n_y$ from 3 to 8, which corresponds to around 40-2000 many-body basis functions in the expansion. Different relative angular momentum states of the two electrons are denoted with $m$.

## 4.3 Basis size

The diagonalization technique for solving few-body wave functions and eigenvalues does not contain any approximations, in principle. But of course the basis size is finite. The convergence can be checked by increasing the number of many-body wave functions in the expansion.

The single-particle basis of the 2D Gaussians of Eq. (4.19) is suitable for closely coupled quantum dots. At large distances and at high magnetic field we expect less accurate results. The accuracy may also depend on the symmetry of the state. For two-electron *parabolic* quantum dot at *zero* magnetic field we can obtain very accurate energy eigenvalues by expanding the basis in relative coordinates. We can test the accuracy of our diagonalization scheme by comparing the energy eigenvalues of the diagonalized matrix to the ones obtained by expanding the wave function in relative coordinates. Fig. 4.1 shows the relative error of energy eigenvalues as a function of the basis size for four different energy eigenstates of two-electron parabolic quantum dot. States with $m = 0, 1, 2, 3$ refer to different relative angular momentum states, where even $m$ are spin-singlet states and odd $m$ spin-triplet states. The relative error is less than one percent for all states

with the smallest basis size and decreases rapidly with increasing basis size. The greatest error is found for the $m = 0$ state. For quantum-dot molecules and finite magnetic field values we cannot make such comparison. The basis size can be, of course, increased and the eigenvalues can be compared to the previous ones until the basis is large enough and the convergence is reached.

Basis size in Fig. 4.1 refers to the number of different exponents $n_x$ and $n_y$ considered in the construction of single-particle states. $n = n_x = n_y$ where $n$ ranges from 3 to 8. For each values of $n_x$ and $n_y$ we can construct $n_x n_y$ different single-particle states and for two electrons we can construct $\binom{n_x n_y}{2} = \frac{(n_x n_y)!}{(n_x n_y - 2)!2!}$ different many-body states. For the spin-singlet we can also have $\phi_i = \phi_j$ or $i = j$ and therefore we have $\frac{(n_x n_y)!}{(n_x n_y - 2)!2!} + n_x n_y$ different many-body states for $S = 0$. For example, with $n = 3$ we have 9 single-particle states and 36 and 45 two-body states for the singlet and triplet states, respectively. For $n = 8$ there are 64 single-particle states and 2016 and 2080 two-body states.

## 4.4 Diagonalization and other computational approaches

In this Thesis we have chosen very accurate exact diagonalization technique as a computational approach for solving the few-body Schrödinger equation for interacting electrons. In the exact diagonalization technique electron-electron interactions and the resulting correlations are taken into account in a correct way, provided that the basis size is sufficient. Correlated many-body states, like fractional quantum Hall states, can be described properly with this method. However, the number of electrons that can be described with a good accuracy with the exact diagonalization technique is very limited as the basis size grows exponentially with the particle number. Therefore, the method is usually restricted to studying less than ten interacting quantum mechanical particles. The diagonalization technique is not either very flexible, as the matrix elements are usually calculated analytically for the system in question. Therefore, when changing something in the Hamiltonian or in the basis functions the new matrix elements must be calculated. Usually it is not so easy to find analytic solutions for the integrals of matrix elements.

To grasp the idea of the limitations of the diagonalization we consider, for example, five and ten electrons, *e.g.*, confined in a quantum dot. Let us assume that $n_{sp} = 10$ and $n_{sp} = 20$ lowest-energy single-particle states are sufficient for describing $N_e = 5$ and $N_e = 10$ electrons accurately, respectively. The corresponding number for many-electron configurations in the many-body expansion, see Eq. (4.11), build from the single-particle states is $\binom{n_{sp}}{N_e} = \frac{n_{sp}!}{(n_{sp} - N_e)!N_e!}$, which

for five electrons is $\binom{10}{5} = 252$ and for ten electrons $\binom{20}{10} = 184756$ and for 20 electrons with 40 single-particle states the many-body basis would include $\binom{40}{20} \approx 10^{11}$ states! Clearly diagonalization of the matrices of the size of $10^{11}$ is not reasonable. The dimensionality can be lowered by the symmetry, but it does not affect the exponential scaling of the basis size.

Twenty electrons, that is already out of the scope of the diagonalization, is not very much in physics and clearly some other computational approaches are needed as well. Due to the basis size limitations and inflexibility of the exact diagonalization technique, other more approximative methods are widely used in describing electrons in quantum dots. One very good wave function method is quantum Monte Carlo, where correlation effects can also be included in a proper way [58, 59]. A very interesting method is a combination between diagonalization and quantum Monte Carlo, see Ref. [60].

More approximative methods include widely used density-functional theory [61, 62] and Hartree-Fock method [63]. Both of these are mean-field methods where electron-electron interactions are taken into account in an averaged way, neglecting the two-body correlations. The original problem of solving Schrödinger equation of interacting electrons is greatly simplified in the mean-field methods allowing greater particle numbers to be considered. Especially the density-functional theory has shown a huge success in condensed matter modeling and theory. One of the founders, Walter Kohn, was awarded with the Nobel Prize in chemistry in 1998. The density-functional theory has shown to be a powerful tool also in modeling two-dimensional quantum dots even with a small number of electrons where the correlation effects are most prominent [64, 65]. However, sometimes mean-field methods cannot provide the correct physical picture [66, 67].

# Chapter 5

# Physical phenomena in quantum-dot molecules

## 5.1 Quantum-dot molecules in a magnetic field

Singlet-triplet splitting, energy levels, magnetization, and wave function analysis of two-electron quantum-dot molecules in a magnetic field are discussed in Publications **III** and **IV**.

A natural step forward from studying individual quantum dots is to couple quantum dots together. Also, in the past, the majority of studies concentrated on individual highly symmetric parabolic quantum dots without disorder. Recently coupling more dots together [68–73] and studying lower symmetry quantum dots [74–78] have gained ground also in the field of quantum dot theory and modeling.

After the Loss and DiVincenzo proposition [20], coupled quantum dots have gained interest due to possible realization as spin-qubit based quantum gates in quantum computing [21, 71, 79]. In addition to coherent single-spin operations, the two-spin operations are sufficient for assembling any quantum computation. Recent experiments have shown a remarkable success in characterizing the few-electron eigenlevels [26, 27, 33], approximating relaxation and time-averaged coherence times and mechanisms [31, 34], and reading single-spin or two-spin states [28, 35] of the quantum dots whereas the coherent manipulation of spin systems remained out of reach until very recent measurements on two-spin rotations [36].

### 5.1.1 Triplet-singlet splitting, energy levels and magnetization

As we have already discussed in the previous chapters, the two-electron wave function can have spin-triplet or spin-singlet ground state, see Eqs. (4.16) and

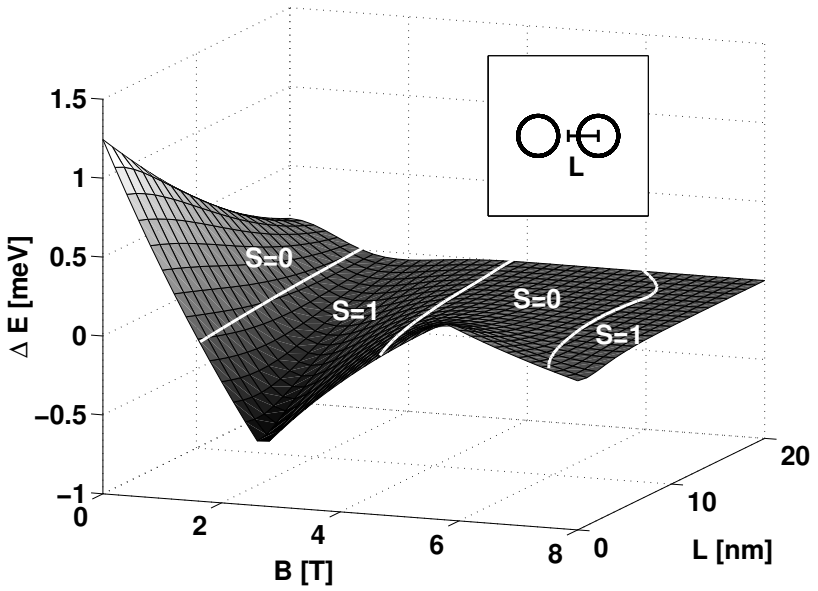


Figure 5.1: Triplet-singlet energy difference $\Delta E = E^{\uparrow\uparrow} - E^{\uparrow\downarrow}$ as a function of magnetic field in two-minima quantum dot molecule. The energy difference is plotted as a function of the dot-dot separation and magnetic field.

(4.17). These spin eigenstates alter as a function of the magnetic field both in a parabolic quantum dot and also in quantum dot molecules [68]. We have calculated the energy difference between the lowest triplet ($S = 1$) and singlet ($S = 0$) states as a function of the magnetic field and the distance between coupled quantum dots for three different quantum-dot molecule confinement potentials. The results are discussed in the Publication **IV**. An example of these in shown in Fig. 5.1. In a weak magnetic field the ground state is a spin singlet, then triplet, and again singlet and triplet. For a finite distance between the dots ($d = 2L$) the energy differences become smaller. We also note that all transition points between singlet and triplet states are shifted to lower $B$ at large distances between the dots.

Fig 5.2 (a) shows a few lowest two-electron energy levels for double double dot with the separation of $d = 2L = 10$ nm between the minima. Dashed lines show the singlet and solid lines the triplet energy levels as a function of the magnetic field. Transitions between singlet and triplet states are seen as crossings of the lowest singlet and triplet energy levels. The excited states show avoided crossings between two levels of a similar symmetry. One interesting anticrossing of two spin singlet states is seen between $B = 2$ and 3 T. We also find anticrossing ground state levels of the two lowest spin triplet states around $B \approx 5$ T, but the repulsion of levels is not so clear at high $B$.

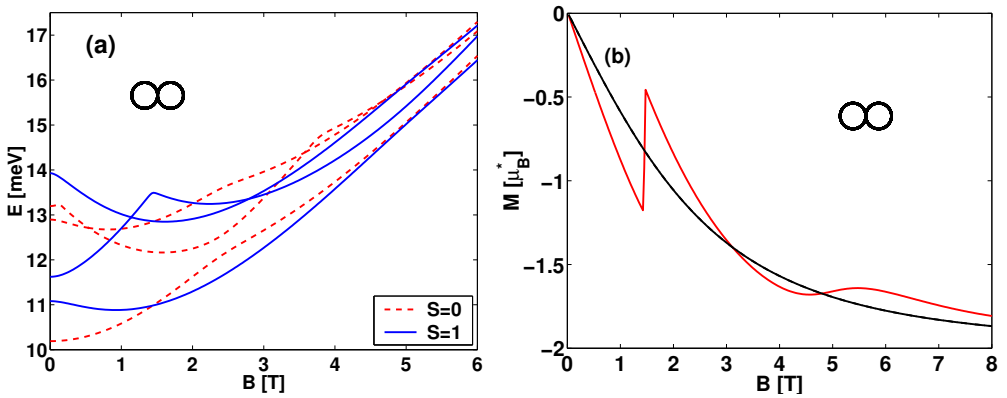


Figure 5.2: (a) the three lowest energy levels of singlet (dashed line) and triplet (solid line) states as a function of magnetic field up to $B = 6$ T for $d = 2L = 10$ nm double dot. Zeeman energy is included in the triplet energies ($E_Z = -2{\times}12.7B[T]$ $\mu$eV in GaAs). (b) magnetization up to $B = 8$ T for $d = 2L = 10$ nm double dot. The smooth curve represents the magnetization of two noninteracting electrons and the other curve shows the magnetization of two interacting electrons. Magnetization is given in the units of effective Bohr magnetons $\mu_B^* = e\hbar/2m^*c$ ($\mu_B^* = 0.87$ meV/T for GaAs).

Another experimentally observable quantity, in addition to the energy levels, is magnetization. The magnetization can be calculated as the derivative of the total energy with respect to magnetic field. It can be divided into to parts, paramagnetic and diamagnetic,

$$M = -\frac{\partial E}{\partial B} = \langle\Psi|\frac{e}{2m^*c}L_z + g^*\mu_B S_z\ |\Psi\rangle - \frac{e^2}{8m^*c^2}\langle\Psi|\sum_i r_i^2|\Psi\rangle B, \qquad (5.1)$$

where the former is constant as a function of the magnetic field, for a given angular momentum and spin state, and the latter depends linearly on the magnetic field. Fig. 5.2 (b) shows the calculated magnetization for $d = 2L_x = 10$ nm double dot. The smooth curve shows magnetization for two noninteracting electrons and the other one for two interacting electrons. The peaks and bumps are only seen with interacting electrons which corresponds to ground state transitions and are identified to paramagnetic response. Both curves show also diamagnetic response to the external magnetic field. This corresponds to increase in the expectation value of the $\langle\Psi|\sum_i r_i^2|\Psi\rangle B$ term of Eq. (5.1). The first sharp jump in the magnetization of the interacting electrons corresponds to the increase in the magnetization as the singlet ground state changes to the triplet. The bump in the magnetization shows how the symmetry of the triplet ground state changes at the avoided crossing point of the two lowest triplet states, see Fig. 5.2 (a) at $B \approx 5$ T.

### 5.1.2 Wave function analysis

There is a lot of informations stored in an accurate few-particle wave function. In a two-electron wave function, if one electron is pinned, the other electron shows a probability distribution depending on the position of the pinned electron. This probability distribution, and also the phase of the conditional wave function, can show a remarkably complex behavior as a function of the magnetic field. These properties of the many-electron wave functions are seldom reproduced correctly by approximative methods. However, recent studies have shown that mean-field methods can reproduce some of the correlation effects surprisingly well [80].

The two-body wave functions of quantum-dot molecules are analyzed by constructing a conditional single-particle wave function:

$$\psi_c(\mathbf{r}) = |\psi_c(\mathbf{r})|e^{i\theta_c(\mathbf{r})} = \frac{\Psi_S[(x,y),(x_2^*,y_2^*)]}{\Psi_S[(x_1^*,y_1^*),(x_2^*,y_2^*)]}, \tag{5.2}$$

where one electron is fixed at position $(x_2^*, y_2^*)$ and the density ($|\psi_c(\mathbf{r})|^2$) and the phase ($\theta_c(\mathbf{r})$) of the other electron can be studied. The most probable positions of electrons $(\mathbf{r}_1^*, \mathbf{r}_2^*)$, are found by maximizing the absolute value of the wave function:

$$\max_{\mathbf{r}_1,\mathbf{r}_2} |\Psi_S(\mathbf{r}_1,\mathbf{r}_2)|^2 \rightarrow \mathbf{r}_1^*, \mathbf{r}_2^*. \tag{5.3}$$

One should note that $\psi_c(\mathbf{r})$ is *not* normalized to result one when integrated over the two-dimensional space because it describes the electron at position $(x, y)$ on the condition that the other electron is fixed at $(x_2^*, y_2^*)$. Instead, $\psi_c(\mathbf{r})$ is normalized to one when $x = x_1^*, y = y_1^*$. Using the conditional single-particle wave function we can study the conditional density $|\psi_c(\mathbf{r})|^2$ and the phase $\theta_c(\mathbf{r})$.

To illustrate how the properties of the many-body wave function can be examined with the conditional single-particle wave function, we compare interacting two-body conditional densities to noninteracting two-body densities in Fig. 5.3. The non-interacting two-body density equals to the single-particle density (up to a normalization). We call it one-body density hereafter. We plot one-body density, two-electron singlet ($S = 0$), and two-electron triplet ($S = 1$) conditional single-particle densities along $x$-axis. The other electron is fixed at the most probable position ($x^*$) on the right hand side of the $x$-axis. Fig. 5.3 (a) and (b) show conditional densities of the single parabolic quantum dot at $B = 1$ and 8 T magnetic fields. One-body density is located at the center since no correlation effects push it towards the edges of the dot. Peak of the triplet state is found further at the edge of the dot than the singlet peak since Pauli exclusion principle ensures that the electrons of the same spin are pushed further apart than the electrons with the opposite spins. Notice that the conditional density of the triplet state goes to zero where the other electron is fixed, just before $x = 20$

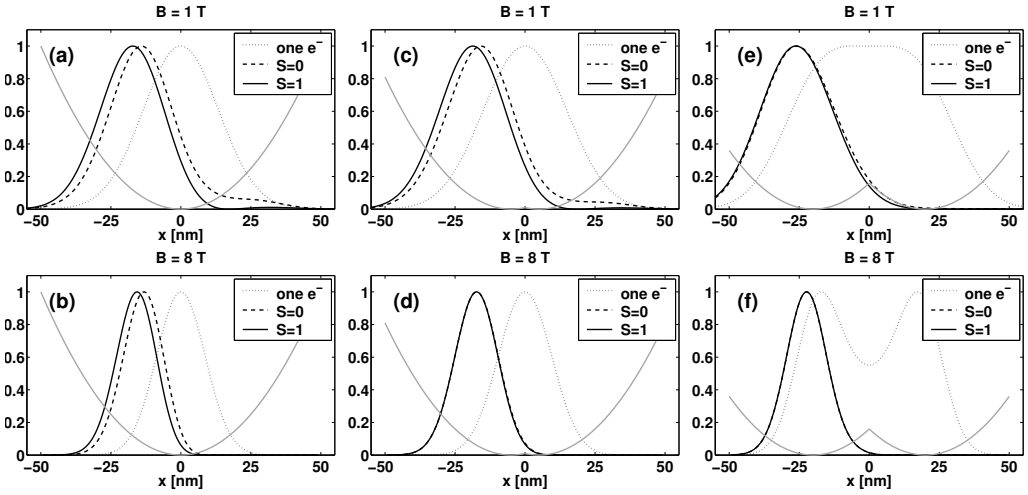


Figure 5.3: One-body density (dotted line), two-body spin-singlet state (dashed line) and two-body spin-triplet state (solid line) along $x$ axis. One of the electrons is fixed at the most probable position in the $x$ axis ($x^*$) and the conditional density is plotted for the other electron ($|\psi_c(\mathbf{r})|^2 = |\Psi_S[(x,y),(x^*,0)]|^2/|\Psi_S[(-x^*,0),(x^*,0)]|^2$). (a) and (b) show the densities of parabolic quantum dot at two different magnetic field values ($B = 1$ and 8 T), (c) and (d) represent double dot with $d = 2L = 10$ nm and (e) and (f) double dot with $d = 2L = 40$ nm. The confinement potential, $V_c$, is plotted with gray color on each figure.

nm, whereas in the singlet state there is a finite probability find the electron around the point of the fixed electron. Fig. 5.3 (c) and (d) show the same data for $d = 2L = 10$ nm double dot, and (e) and (f) for $d = 2L = 40$ nm double dot. At high magnetic fields and large dot-dot separations the difference between singlet and triplet densities reduces. At large distances between the dots and at high magnetic field also the one-body density localizes into the individual dots, see Fig. 5.3 (f).

When the angular momentum increases, the increased rotation induces vortices in the system. As we have a many-body system, the rotation is a correlated motion of electrons and can be studied in the relative coordinates of electrons. Vortices can be found by locating the zeros of the wave function and studying the phase of the wave function when going around each of the zeros. As the vortices are seen in the relative coordinates, and are not visible in the density, we examine the conditional single-particle wave function $\psi_c(\mathbf{r})$ (of Eq. (5.2)), where one electron is fixed in the most probable position. The vortices are seen in the zeros of $\psi_c$. When the phase part, $\theta_c$, is integrated around a closed path encircling the zero, we obtain the winding number $m$ of a vortex ($\oint \theta_c(\mathbf{r}) d\mathbf{r} = m2\pi$).

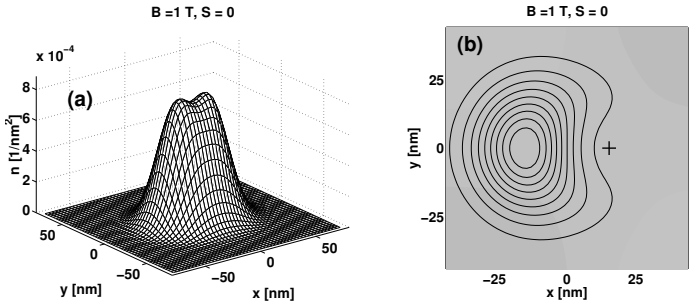


Figure 5.4: $d = 2L = 10$ nm double dot spin-singlet state at $B = 1$ T. (a) shows total electron density and (b) contours of conditional density $|\psi_c(\mathbf{r})|^2$ with the other electron fixed at the most probable position, marked with + sign.

To show how the complex many-electron effects appear in the wave functions of quantum-dot molecules, we examine also the phase of the conditional wave function. Fig. 5.4 shows the double dot (with $d = 2L = 10$) total electron density in (a) and the contours of conditional density and the phase in gray background color in (b) for spin-singlet state at $B = 1$ T. Fig. 5.5 shows the total electron density in (a), the phase of the conditional wave function and contours of conditional density in (b) and vortices of the conditional wave function with the fixed electrons at three different positions in (c) with contours of the *total* electron density in the background for spin-triplet state of $d = 2L = 10$ nm double dot at $B = 7.5$ T. The total electron density can be obtained by integrating one variable out from the two-body wave function $n(\mathbf{r}_1) = \int d\mathbf{r}_2 |\Psi_S(\mathbf{r}_1, \mathbf{r}_2)|^2$.

Figs. 5.4 (b) and 5.5 (b) show the ground state contours of the conditional electron density $|\psi_c|^2$ for the same double dot at two different magnetic field values, $B = 1$ and 7.5 T, respectively. The gray-scale background in Figs. 5.4 (b) and 5.5 (b) marks the phase of the conditional wave function, $\theta_c$, where the white color equals $\theta_c = 0$ and the darkest gray $\theta_c = 2\pi$. The positions of the vortices are marked with circles (o), and the other electron is fixed at the most probable position ($\mathbf{r}_2^*$) shown with a plus sign (+). The lines of dark gray and white borders correspond to a sudden phase change of $2\pi$ if the line is crossed. The number of flux quanta attached to the electron (or the winding number of a vortex) can be determined by going around the fixed electron position and calculating the total phase change (or counting the lines crossed in the figure).

For the low-field singlet in Fig. 5.4 (b) the phase is constant and no vortices are found in the vicinity of the fixed electron. Fig. 5.5 (b), on the other hand, show a very complex structure of three vortices in the vicinity of the fixed electron. This type of wave function resembles Laughlin wave function [81], but as there is a repulsion between the vortices it is even more complicated. These vortices follow the fixed electron if its position is changed, as can be seen in Fig. 5.5 (c), where

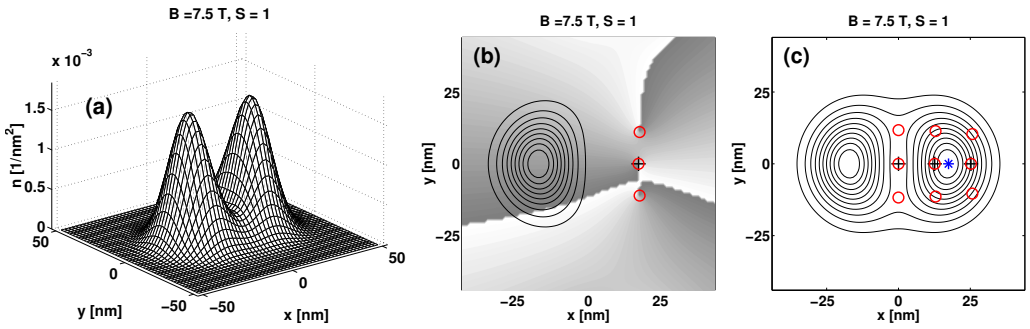


Figure 5.5: $d = 2L = 10$ nm double dot spin-triplet state at $B = 7.5$ T. (a) shows the total electron density and (b) the contours of the *conditional* density $|\psi_c(x, y)|^2$ and phase of the conditional wavefunction $\theta_c(x, y)$ in gray-scale. (White equals $\theta_c = 0$ and darkest gray $\theta_c = 2\pi$). The plus sign (+) indicates the position of the fixed electron and small circles indicate the positions of the vortices. In (c) contours of the *total* electron density are plotted in the background and positions of the vortices are solved when the fixed electron is in three different positions. Fixed electron is marked with the plus sign and vortices with circles. The most probable position is marked with a star.

the electron is fixed at three different positions and three vortices are following aside. This is a signature of composite particles of electrons and vortices [82].

## 5.2 Far-infrared spectrum

Magneto-optical absorption spectrum in the far-infrared (FIR) range of quantum dot molecules is discussed in Publications **II**, **III** and **V**.

Far-infrared (FIR) magneto-optical absorption spectroscopy is one of the experimental techniques to study electrons confined in semiconductor quantum dots [4, 47]. It was, however, realized at the early stage of quantum dot research that the FIR spectroscopy is unable to reveal interesting many-electron effects in parabolic-confinement quantum dots. This is because the electromagnetic waves couple only to the center-of-mass variables of electrons. The resulting FIR spectrum is rather simple, showing two branches, $\omega_\pm$, as a function of magnetic field [44, 45]. These branches, one with positive energy dispersion ($\omega_+$) and one with negative energy dispersion ($\omega_-$) as a function of magnetic field, are called the Kohn modes. The spectrum does not depend on the number of electrons nor on the interactions between them. This condition in parabolic quantum dots is called generalized Kohn theorem [43]. The condition can be lifted if the confinement is not parabolic and many experiments show more complex FIR

spectra [46–49]. Also calculations [83–88] have shown non-trivial FIR spectra of non-parabolic quantum dots. It is also possible that spin-orbit interaction [89] and impurities near quantum dots [90] can have an effect on the FIR spectrum. In a nonparabolic quantum dot, the internal relative motion of electrons could be accessible with FIR spectroscopy, but our studies in Publications **II**, **III** and **V** suggest that the additional features in the FIR spectra are still of collective nature. The interpretation of observed FIR spectra of a nonparabolic quantum dot is usually far from trivial. It is clear that the deviations arise from nonparabolic confinement, but the detailed cause of the deviations, thus the interpretation of spectrum, is not always straightforward. It is especially interesting to see how many-electron interactions appear in the FIR spectra of quantum dots.

### 5.2.1 Far-infrared spectra of quantum-dot molecules

In the calculation of FIR spectra of two interacting electrons we use exact diagonalization technique to obtain two-electron wave functions. Dipole-transition probabilities are calculated with perturbation theory between the two-body levels. The FIR spectrum is calculated as transition probabilities from ground state ($E_0$) to excited states ($E_l$) using the Fermi golden rule within the electric-dipole approximation:

$$\mathcal{A}_{l\pm} \propto \left| \left\langle \Psi_l \left| e^{\pm i\phi} \sum_{i=1}^{2} \mathbf{r}_i \right| \Psi_0 \right\rangle \right|^2 \delta(E_l - E_0 - \hbar\omega). \tag{5.4}$$

We assume circular polarization of the electromagnetic field: $e^{\pm i\phi} \sum_i \mathbf{r}_i = \sum_i (x_i \pm iy_i) = z_\pm$, where plus indicates right-handed polarization and minus left-handed polarization. The results are presented for non-polarized light as an average of the two circular polarizations.

The dipole-allowed magneto-optical excitation spectrum of an isolated harmonic-confined quantum dot consist of two branches $\omega_+$ and $\omega_-$, whose energy dispersion is well understood and it does not depend on the number of electrons in the quantum dot:

$$\Delta E_\pm = \hbar\omega_\pm = \hbar\sqrt{\omega_0^2 + (\omega_c/2)^2} \pm \hbar\omega_c/2. \tag{5.5}$$

$\omega_0$ describes the external confinement, $\omega_c = eB/m^*$ is the cyclotron frequency, and $m^*$ is the effective mass of electron. In the dipole-allowed transitions between Fock-Darwin states angular momentum must change by unity, $\Delta l = \pm 1$.

For a two-electron quantum dot the ground state can be either spin singlet ($S = 0$) or spin triplet ($S = 1$) depending on the magnetic field strength. Even if many-body energy levels have more complicated magnetic field dispersion than the single-particle levels, the dipole-transitions in the many-body case always

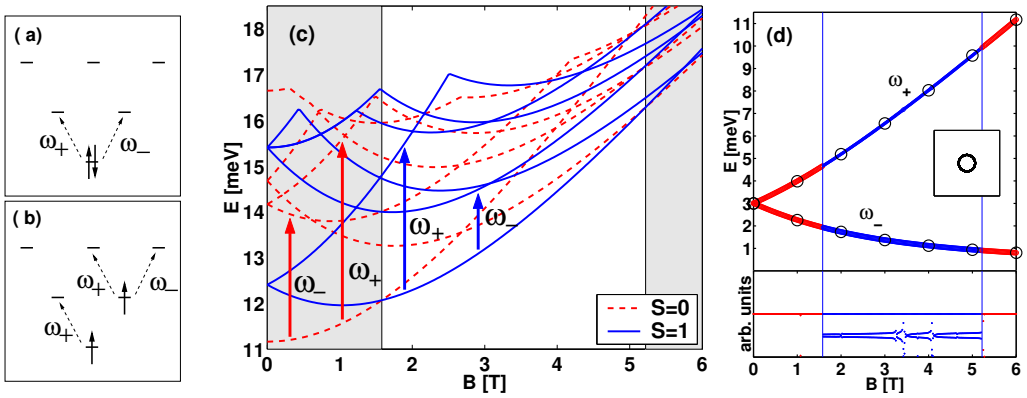


Figure 5.6: (a) and (b): schematic picture of transitions at zero magnetic field for the spin-singlet and spin-triplet states of a parabolic quantum dot, respectively. (c) energy levels of a two-electron parabolic quantum dot as function of magnetic field. (d) far-infrared spectrum of a parabolic quantum dot.

equal to transitions between the single-particle levels, in a *parabolic* confinement. A schematic picture of transitions at zero magnetic field is shown in Fig. 5.6 (a) and (b) for spin-singlet and spin-triplet states, respectively. Fig. 5.6 (c) shows few lowest two-body energy levels as a function of magnetic field for the singlet and triplet states of a parabolic quantum dot. Gray background marks the magnetic field region of spin-singlet ground state and white spin-triplet ground state. Dipole transitions from one spin type to another are forbidden.

Fig. 5.6 (d) shows the calculated FIR spectra for two interacting electrons in a parabolic quantum dot. The dipole transition probabilities are calculated from the two-body ground state level to higher two-body energy levels as shown in Fig. 5.6 (c). The energy of absorbed light is given in meV as a function of magnetic field. The width of the line is proportional to the transition probability, which is also plotted below the spectrum (in arbitrary units) for each of the branches in the spectrum. There are, of course, many more possible transitions with zero or small probability. Only the lines with transitions probability exceeding one percent of the maximum transition probability are included in Fig. 5.6 (d). Large open circles in the spectra represent two Kohn modes, $\omega_+$ and $\omega_-$, plotted with one tesla spacings. Vertical lines indicate the singlet-triplet (or triplet-singlet) transition points.

Fig. 5.7 shows the calculated FIR absorption spectra for two interacting electrons in quantum-dot molecules. Fig. 5.7 (a) shows FIR spectrum for two-minima quantum-dot molecule (double dot), (b) for square symmetric four-minima quantum-dot molecule and (c) for rectangular-symmetric four-minima quantum-dot molecule. Now as the symmetry of the confining potential is lower, we observe some ad-

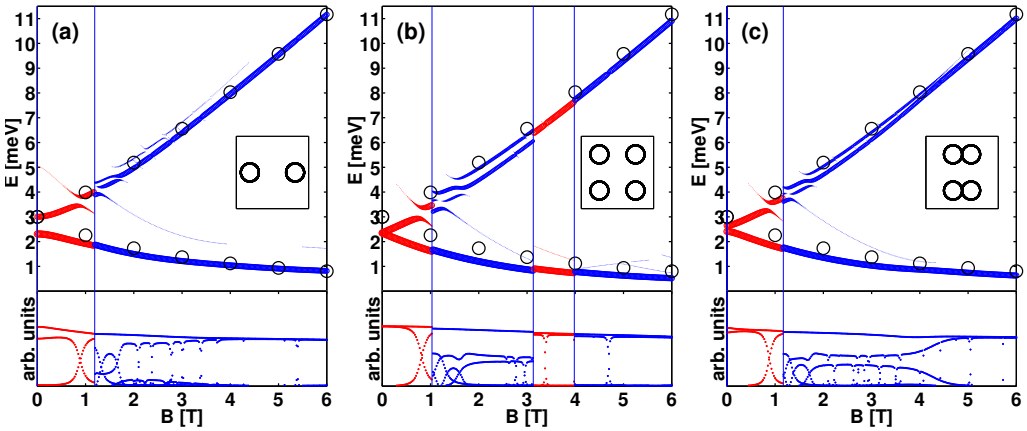


Figure 5.7: Far-infrared spectra of quantum-dot molecules. (a) for $L_x = 15, L_y = 0$ nm double dot, (b) for $L_x = L_y = 10$ nm four-minima quantum-dot molecule and (c) for $L_x = 5, L_y = 10$ nm rectangular-symmetric four-minima quantum dot molecule.

ditional features in the FIR spectra. Detailed analysis of the FIR spectra of quantum-dot molecules is presented in Publications **II**, **III** and **V**.

## 5.3 Classical many-electron states

Classical many-electron states and their quantum-mechanical counterparts are discussed in Publication **I**.

In the limit of weak confinement (low density) or a very strong magnetic field the quantum effects are quenched and the electron correlations start to dominate the properties of the system. There is a theoretical evidence for the existence of a limit where the electron system crystallizes to Wigner molecules, which is seen as the localization of the electron density around positions that minimise the Coulomb repulsion [91–99]. The ultimate limit is a purely classical system where only the Coulomb repulsion between the electrons defines the ground state. The problem reduces to finding the classical positions of electrons that minimise the total energy of the system. One should also note as pointed out by Harju *et al.* [97], based on accurate quantum mechanical calculations, that a correlated many-electron system in a quantum dot can well be described in terms of independent electrons oscillating around their classical positions. This picture is energetically very accurate far beyond the confinement values where the system shows Wigner-molecule-like behavior.

The classical limit of electrons confined in a quantum dot is achieved by setting $\hbar$ to zero, thus neglecting the kinetic energy of the electrons. The problem reduces

to finding the positions of point charges in the parabolic confinement that minimise the total energy. The $1/r$ Coulomb repulsion pushes electrons apart while the parabolic confinement favours electrons to be as close as possible to the centre of the harmonic dot. The positions for two, three, and maybe four electrons in a dot can be predicted from the form of the Hamiltonian quite easily, but for more particles in the dot the problem is not trivial at all. The classical point charges in a two-dimensional infinite plane crystallise into a hexagonal lattice at low temperatures. Parabolic confinement, on the other hand, favours circular symmetric solutions. In parabolic quantum dots these two effects, the circular symmetry and the formation of a hexagonal lattice, compete, thus resulting in non-trivial electron clusters.

The ground state configurations of a single parabolic quantum dot with classical point charges have been studied previously [100–102]. Large systems (N > 200) exhibit a clear triangular lattice structure in the inner part of the dot and a shell-like structure at the outer edge. With the small number of particles in the dot the shell structure is more pronounced. A vertically coupled parabolic two-dot system was studied by Partoens *et al.* [103]. Several structural transitions as a function of the distance between dots were found. In this Thesis, in Publication **I**, we present a study of classical point charges in *laterally* coupled parabolic dots and study the ground state and metastable (local minimum) configurations and structural transitions as a function of the inter-dot distance.

### 5.3.1 Monte Carlo simulation

The classical electrons in the double dot are modelled with the classical Hamiltonian of the following form

$$H = \frac{1}{2}\, m^* \omega_0^2 \sum_{i=1}^{N} \min\left[(\vec{r}_i - d/2)^2, (\vec{r}_i + d/2)^2\right] + \frac{e^2}{4\pi\epsilon_0\epsilon} \sum_{i<j} \frac{1}{|\vec{r}_i - \vec{r}_j|}. \quad (5.6)$$

Each one of the $N$ electrons is described with coordinates $\vec{r}_i = (x_i, y_i)$ in the two-dimensional space. The harmonic confinements are positioned symmetrically around the origin with distance $d = 2L_x$ between the minima of the confinements. We measure the energy in meV's and distance in Ångströms. The confinement strength was set to $\hbar\omega_0 = 3$ meV and typical GaAs parameters were chosen to the effective mass and the dielectric constant: $m^* = 0.067\ m_e$ and $\epsilon = 13$.

The minimum energy as a function of the positions of the particles, $E_{tot} = \min\ E(\vec{r}_1, ..., \vec{r}_N)$, is solved with a standard Metropolis Monte Carlo method [104]. Starting from a randomly chosen initial configuration $\vec{r}_1, ..., \vec{r}_N$ we start displacing one particle at time. A trial movement is accepted if the total energy of the

system is reduced. If the energy is increased, the step is accepted with the probability $e^{-\Delta E\beta}$, where $\Delta E$ is the change in energy between the trial and previously accepted configuration. $\beta = 1/kT_{eff}$ plays the role of the effective (inverse) temperature. When $\beta$ is very small compared to the typical energy change ($\Delta E$) in the simulation, the probability of accepting any step is high and particles are moving in random directions. A high value of $\beta$, and thus small effective temperature, favors steps that move towards a minimum in the energy surface. The direction of the trial step is chosen randomly and the two coordinates, $x$ and $y$, both between -0.5 and 0.5, are multiplied by the chosen maximum movement $R_{max}$. The simulation is started with high effective temperature (small $\beta$) and large $R_{max}$. Particles move in random directions with long steps. During the run $R_{max}$ is reduced and $\beta$ increased. At the end particles are nearly frozen around the minimum energy positions and the energy does not change considerably. Thus we have obtained the minimum in energy. The Monte Carlo simulation can also converge to a metastable state. In order to find the absolute minimum, the minimization is performed many times. We also gain interesting information of the metastable configurations.

### 5.3.2 Transitions in electron configurations

As the distance between the two dots, $d$, increases, we observe structural transitions in the electron configurations. At $d = 0$ we have just one dot and when the dots are infinitely apart, $d \to \infty$, the system consist of two independent dots. It is clear, that when the confining potential changes with increasing $d$, also the minimum energy positions of the electrons must be modified. We find the changes in the electron configurations to exhibit surprisingly complex behavior as a function of the distance between the dots.

We mark electron configurations with (nearly) concentric shells around the potential minimum: $(N_1, N_2)$, where $N_1$ denotes the number of electrons in the innermost shell and $N_2$ the electrons in the outermost the shell. The clearest example of a transition can be seen for six electrons between $d = 0$ and $d = 200$ Å, see Fig. 5.8. At $d = 0$ the (1,5) configuration is the ground state and (6) the metastable state. At $d = 200$ Å it is the other way around: (6) is the ground and (1,5) a metastable state. The energy as a function of distance for two alternative configurations is shown in Fig. 5.8(a). The transition point, marked with a small circle, is at $d = 111.6$ Å. For $N = 8$, we find that at $d = 135.9$ Å the electron configuration changes from (1,7) to (2,6), see Fig. 5.8 (b). Notice that the (2,6) configuration is not stable at $d = 0$ and it is unstable for $d \lesssim 17$ Å.

To show that the classical transitions are relevant even for the quantum case, we have studied the non-interacting quantum-mechanical $N = 6$ case. The non-interacting quantum mechanical problem can be reduced to a one dimensional

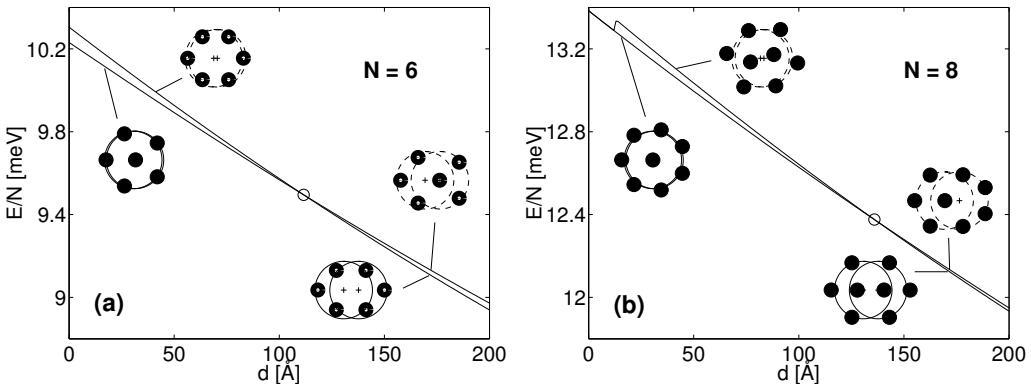


Figure 5.8: Energy per particle as a function of distance for $N = 6$ and $N = 8$ classical electrons in lateral double dot. The small circles indicate the discontinuous structural transition points.

one as the potential is separable, and the single-particle states of the transverse motion ($y$ direction) are those of the simple harmonic oscillator with energy $\varepsilon_{n_\mathrm{y}} = \frac{1}{2} + n_\mathrm{y}$, where $n_\mathrm{y} = 0, 1, 2, \ldots$. The one-dimensional longitudinal part can easily be solved numerically. Combining the energies of the longitudinal part with the transverse ones, one obtains the spectra of Fig. 5.9. One can see that the energies are equal to those of the simple harmonic oscillator for $d = 0$, and of two independent oscillators at large $d$. In the quantum mechanical limit we measure the length in units of $l_0 = \sqrt{\hbar/m^*\omega}$ and energy in units of $\hbar\omega$. One can also estimate the coupling between the two dots in Fig. 5.9. At $d \approx 1.5l_0$ energy of the lowest eigen state is at the minimum whereas at $d \approx 4l_0$ the lowest bonding and antibonding states are already very close in energy, which means that dots rather decoupled. For higher energy states the electron density is relaxed more outwards and therefore the bonding and antibonding states combine at a greater distance between the dots. Coupling depends also on the occupied level.

We drop the spin of the quantum mechanical electrons, as it is not relevant in the classical limit. This corresponds to taking the system to be spin-polarized. We occupy the six lowest eigen states with spinless electrons. One can see from the energy levels shown in Fig. 5.9 that there exists one transition for $N = 6$ electrons. In this transition point, one electron moves from a bonding $n_\mathrm{y} = 2$ state to an antibonding $n_\mathrm{y} = 0$ state. In the classical limit, the electrons avoid each other due to the Coulomb interaction. In our noninteracting quantum mechanical case, the electron-electron repulsion results from the Pauli principle.

When the quantum mechanical system approaches the classical limit, the most probable configuration $\mathbf{R}^*$, maximizing the density $|\Psi(\mathbf{R})|^2$ approaches the classical electron positions. The quantum effects and the transition to the classical

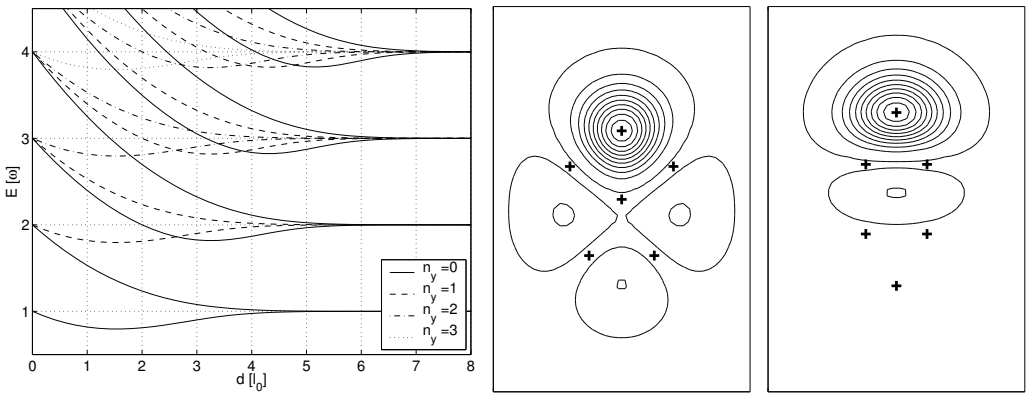


Figure 5.9: Left: Lowest single-particle energies as a function of the interdot distance $d$. The inset shows the quantum number of the transverse motion. Middle and Right: Conditional probability densities and the most probable electron positions (marked with plus signs). The middle (right) panel corresponds to small (large) interdot distance $d$, correspondingly. The contours are uniformly from 0.01 to 0.91.

limit are most conveniently studied using the single-particle probability distribution $\tilde{\rho}(\mathbf{r})$ [97], defined as

$$\tilde{\rho}(\mathbf{r}) = \left| \frac{\Psi(\mathbf{r}, \mathbf{r}_2^*, \ldots, \mathbf{r}_N^*)}{\Psi(\mathbf{r}_1^*, \mathbf{r}_2^*, \ldots, \mathbf{r}_N^*)} \right|^2 , \tag{5.7}$$

where the coordinates $\mathbf{r}_i^*$ are fixed to the ones from the most probable configuration $\mathbf{R}^*$. In approaching the classical limit, the density $\tilde{\rho}(\mathbf{r})$ is more and more peaked around the classical position $\mathbf{r}_1^*$, still showing quantum fluctuations, as seen in the case of a single quantum dot [97].

We now take the quantum model of six electrons to the opposite limit than the classical one where the information of the classical positions might be stored in the coordinates of the most probable electron configuration. One can see in Fig. 5.9, which shows the $\tilde{\rho}(\mathbf{r})$ for the two ground states that this is really the case. It is very interesting to see that the most probable electron positions change in the transition point very similarly to the classical case. We see clearly a similar transition as with classical electrons. It is highly non-trivial that the electron triangles for the large-$d$ case are facing the same way as in the classical case. Our quantum mechanical analysis of the $N = 6$ case shows that these type of transitions are very relevant for quantum-dot molecules also beyond the classical limit.

# Chapter 6

# Summary

In this Thesis the properties of few-electron laterally coupled quantum dots or quantum-dot molecules have been modeled. Emphasis has been on describing electron correlations properly. We have mostly considered two interacting electrons confined in quantum-dot molecules. These two-electron quantum states show a remarkably complex behavior as a function of magnetic field. We have analyzed the effects of electron correlations and quantum dot confinement on energy levels, magnetization, and far-infrared magneto-optical absorption spectra of quantum-dot molecules. In addition, classical few-electron states in quantum-dot molecules were also discussed in this Thesis.

In Publication **I**, we studied classical point charges confined in a lateral double dot system. Classical electrons show structural transitions in the ground-state and metastable configurations as a function of the inter-dot distance. We have also identified a similar structural transition in the wave function of six noninteracting quantum mechanical electrons.

Publications **II**, **III** and **V** discuss far-infrared magneto-optical absorption spectra of quantum-dot molecules. The effects of the confinement potential and the electron interactions have been analyzed in detail. We conclude that the two-electron far-infrared spectra directly reflect the symmetry of the confinement potential, and the interactions cause only small shifts in the spectra. We suggest that these shifts could be tested in experiments by varying the number of electrons confined in quantum dots.

Publications **III** and **IV** present results for two-electron quantum-dot molecules in a magnetic field. We have studied ground state transitions as a function of the distance between the dots and as a function of magnetic field. All quantum-dot molecule confinements show transitions between spin-singlet and spin-triplet ground states as a function of the magnetic field. The states in a high magnetic

field can be identified as composite particles of electrons and vortices. We observe avoided level crossings in the spectra of the quantum-dot molecules. The anticrossings can be observed in the low-lying energy states and in the magnetization.

As a general conclusion, few-electron states of lateral quantum dot molecules show a rich and complex behavior as a function of the tunable system parameters. Classical electron configurations of a double dot system show complex transitions as a function of the separation between the dots. We have analyzed the two-electron quantum states in quantum-dot molecules in a magnetic field and a find complex spin-phase diagram and composite particles of electrons and vortices. This type of two-electron states of a double quantum dot device may be building blocks for spin qubits in future quantum computing. Furthermore, we have shown that the far-infrared magneto-optical absorption spectra mainly reflect the low symmetry of the quantum dot confinement potential and interactions cause only small shifts in the spectra.

# Bibliography


[1] M. A. Kastner, *Artificial atoms*, Physics Today **46**, 24 (1993).

[2] R. Ashoori, *Electrons in artificial atoms*, Nature **379**, 413 (1996).

[3] L. Kouwenhoven and C. Marcus, *Quantum dots*, Physics World **11**, 35 (1998).

[4] L. Jacak, P. Hawrylak, and A. Wójs, *Quantum Dots* (Springer, 1998).

[5] T. Chakraborty and P. Pietiläinen, *The Quantum Hall Effects: Fractional and Integral* (Springer, Berlin, 1995).

[6] T. H. Oosterkamp, J. W. Janssen, L. P. Kouwenhoven, D. G. Austing, T. Honda, and S. Tarucha, *Maximum-density droplet and charge redistributions in quantum dots at high magnetic fields*, Phys. Rev. Lett. **82**, 2931 (1999).

[7] M. P. Schwarz, D. Grundler, M. Wilde, C. Heyn, and D. Heitmann, *Magnetization of semiconductor quantum dots*, J. Appl. Phys. **91**, 6875 (2002).

[8] M. P. Schwarz, D. Grundler, C. Heyn, D. Heitmann, , D. Reuter, and A. Wieck, *Induced nonequilibrium currents in the magnetization of mesoscopic dots in the quantum Hall regime*, Phys. Rev. B 68 **68**, 245315 (2003).

[9] S. Ilani, J. Martin, E. Teitelbaum, J. H. Smet, D. Mahalu, and V. U. A. Yacoby, *The microscopic nature of localization in the quantum Hall effect*, Nature **427**, 328 (2004).

[10] H. Saarikoski, E. Räsänen, A. Harju, and M. Helle, *Magnetization of large quantum dots: de Haas-van Alphen effect and signatures of vortex formation*, unpublished (2005).

[11] C. Beenakker and C. Schönenberger, *Quantum shot noise*, Physics Today **56**, 37 (2003).

[12] J. Aghassi, A. Thielmann, M. Hettler, and G.Schön, *Strongly enhanced shot noise in chains of quantum dots* (2005), cond-mat/0505345.

[13] C. Livermore, C. H. Crouch, R. M. Westervelt, K. L. Campman, and A. C. Gossard, *The Coulomb blockade in coupled quantum dots*, Science **274**, 1332 (1996).

[14] T. H. Oosterkamp, T. Fujisawa, W. G. van der Wiel, K. Ishibashi, R. V. Hijman, S. Tarucha, and L. P. Kouwenhoven, *Microwave spectroscopy of a quantum dot molecule*, Nature **395**, 873 (1998).

[15] M. Brodsky, N. B. Zhitenev, R. C. Ashoori, L. N. Pfeiffer, and K. W. West, *Localization in artificial disorder: two coupled quantum dots*, Phys. Rev. Lett. **85**, 2356 (2000).

[16] A. W. Holleitner, R. H. Blick, A. K. Hüttel, K. Eberl, and J. P. Kotthaus, *Probing and controlling the bonds of an artificial molecule*, Science **297**, 70 (2002).

[17] W. G. van der Wiel, S. D. Franceschi, M. Elzerman, T. Fujisawa, S. Tarucha, and L. P. Kouwenhoven, *Electron transport through double quantum dots*, Rev. Mod. Phys. **75**, 1 (2003).

[18] T. Hatano, M. Stopa, T. Yamaguchi, T. Ota, K. Yamada, and S. Tarucha, *Electron-spin and electron-orbital dependence of the tunnel coupling in laterally coupled double vertical dots*, Phys. Rev. Lett. **93**, 066806 (2004).

[19] D. P. DiVincenzo, *Quantum computation*, Science **270**, 255 (1995).

[20] D. Loss and D. P. DiVincenzo, *Quantum computation with quantum dots*, Phys. Rev. A **57**, 120 (1998).

[21] G. Burkard, D. Loss, and D. P. DiVincenzo, *Coupled quantum dots as quantum gates*, Phys. Rev. B **59**, 2070 (1999).

[22] J. M. Taylor, H.-A. Engel, W. Dür, A. Yacoby, C. M. Marcus, P. Zoller, and M. D. Lukin, *Fault-tolerant architecture for quantum computation using electrically controlled semiconductor spins*, Nature Physics **1**, 177 (2005).

[23] D. P. DiVincenzo, *The physical implementation of quantum computation*, Fortschr. Phys. **48**, 771 (2000).

[24] J. M. Elzerman, R. Hanson, L. H. W. van Beveren, B. Witkamp, J. S. Greidanus, R. N. Schouten, S. D. Franceschi, S. Tarucha, L. M. K. Vandersypen, and L. Kouwenhoven, *Quantum Dots: a Doorway to Nanoscale Physics* (Springer, Berlin, 2005), vol. 667 of *Lecture Notes in Physics*, chap. Semiconductor few-electron quantum dots as spin qubits.

[25] H.-A. Engel, L. P. Kouwenhoven, D. Loss, and C. M. Marcus, *Controlling spin qubits in quantum dots*, Quantum Information Processing **3**, 115 (2004), cond-mat/0409294.

[26] S. D. Lee, S. J. Kim, J. S. Kang, Y. B. Cho, J. B. Choi, S. Park, S.-R. E. Yang, S. J. Lee, and T. H. Zyung, *Spin singlet-triplet transition in a Si-based two-electron double quantum dot molecule* (unpublished), cond-mat/0410044.

[27] J. M. Elzerman, R. Hanson, J. S. Greidanus, L. H. W. van Beveren, S. D. Franceschi, L. M. K. Vandersypen, S. Tarucha, and L. P. Kouwenhoven, *Few-electron quantum dot circuit with integrated charge read out*, Phys. Rev. B **67**, 161308(R) (2003).

[28] J. M. Elzerman, R. Hanson, L. H. W. van Beveren, B. Wilfkamp, L. M. K. Vandersypen, and L. P. Kouwenhoven, *Single-shot read-out of an individual electron spin in a quantum dot*, Nature (London) **430**, 431 (2004).

[29] D. M. Zumbühl, C. M. Marcus, M. P. Hanson, and A. C. Gossard, *Cotunneling spectroscopy in few-electron quantum dots*, Phys. Rev. Lett. 93 **93**, 256801 (2004).

[30] J. Elzerman, R. Hanson, J. Greidanus, L. W. van Beveren, S. DeFranceschi, L. Vandersypen, S. Tarucha, and L. Kouwenhoven, *Tunable few-electron double quantum dots with integrated charge read-out*, Physica E 25 **25**, 135 (2004).

[31] A. C. Johnson, J. R. Petta, J. M. Taylor, A. Yacoby, M. D. Lukin, C. M. Marcus, M. P. Hanson, and A. C. Gossard, *Triplet-singlet spin relaxation via nuclei in a double quantum dot*, Nature **435**, 925 (2005), cond-mat/0503687.

[32] T. Hatano, M. Stopa, and S. Tarucha, *Single-electron delocalization in hybrid vertical-lateral double quantum dots*, Science **309**, 268 (2005).

[33] A. K. Hüttel, S. Ludwig, H. Lorenz, K. Eberl, and J. P. Kotthaus, *Direct control of the tunnel splitting in a one-electron double quantum dot*, Phys. Rev. B **72**, 081310(R) (2005).

[34] F. H. L. Koppens, J. A. Folk, J. M. Elzerman, R. Hanson, L. H. W. van Beveren, I. T. Vink, H. P. Tranitz, W. Wegscheider, L. P. Kouwenhoven, and L. M. K. Vandersypen, *Control and detection of singlet-triplet mixing in a random nuclear field*, Science **309**, 1346 (2005), published online 27 July 2005 (10.1126/Science.1113719).

[35] R. Hanson, I. T. V. L. H. Willems van Beveren, J. M. Elzerman, W. J. M. Naber, L. P. K. F. H. L. Koppens, and L. M. K. Vandersypen, *Single-shot readout of electron spin states in a quantum dot using spin-dependent tunnel rates*, Phys. Rev. Lett. **94**, 196802 (2005).

[36] J. R. Petta, A. C. Johnson, J. M. Taylor, E. A. Laird, A. Yacoby, M. D. Lukin, C. M. Marcus, M. P. Hanson, and A. C. Gossard, *Coherent manipulation of coupled electron spins in semiconductor quantum dots*, Science **309**, 2180 (2005), published online 1 September 2005 (10.1126/science.1116955).

[37] D. P. DiVincenzo, *Double quantum dot as a quantum bit*, Science **309**, 2173 (2005).

[38] S. Datta, *Electron Transport in Mesoscopic Systems* (Cambridge University Press, 1997).

[39] D. Bimberg, M. Grundmann, and N. N. Ledentsov, *Quantum Dot Heterostructures* (Wiley, Chichester, 1999).

[40] S. Farad, K. Hinzer, S. Raymond, M. M. Dion, J. P. Caffrey, Y. Feng, and S. Charbonneau, *Red-emitting semiconductor quantum dot lasers*, Science **274**, 1350 (1996).

[41] L. P. Kouwenhoven, T. H. Oosterkamp, M. W. S. Danoesastro, M. Eto, D. G. Austing, T. Honda, and S. Tarucha, *Excitation spectra of circular few-electron quantum dots*, Science **278**, 1788 (1997).

[42] W. G. van der Wiel, S. D. Franceschi, J. M. Elzerman, T. Fujisawa, S. Tarucha, and L. P. Kouwenhoven, *Electron transport through double quantum dots*, Rev. Mod. Phys. **75**, 1 (2003).

[43] P. A. Maksym and T. Chakraborty, *Quantum dots in a magnetic field: Role of electron electron interactions*, Phys. Rev. Lett. **65**, 108 (1990).

[44] C. Sikorski and U. Merkt, *Spectroscopy of electronic states in InSb quantum dots*, Phys. Rev. Lett. **62**, 2164 (1989).

[45] B. Meurer, D. Heitmann, and K. Ploog, *Single-electron charging of quantum-dot atoms*, Phys. Rev. Lett. **68**, 1371 (1992).

[46] T. Demel, D. Heitmann, P. Grambow, and K. Ploog, *Nonlocal level crossings in quantum dot structures*, Phys. Rev. Lett. **64**, 788 (1990).

[47] D. Heitmann and J. P. Kotthaus, *The spectroscopy of quantum dot arrays*, Physics Today **June**, 56 (1993).

[48] M. Hochgräfe, C. Heyn, and D. Heitmann, *Intersection and anticrossing of far-infrared modes in elliptical quantum dots with tunable ellipticity*, Phys. Rev. B **63**, 035303 (2001).

[49] R. Krahne, V. Gudmundsson, C. Heyn, and D. Heitmann, *Far-infrared excitations below the Kohn mode: Internal motion in a quantum dot*, Phys. Rev. B (2001).

[50] M. P. Schwarz, M. A. Wilde, S. Groth, D. Grundler, C. Heyn, and D. Heitmann, *Sawtoothlike de Haas-van Alphen oscillations of a two-dimensional electron system*, Phys. Rev. B **65**, 245315 (2002).

[51] T. H. Oosterkamp, S. F. Godijn, M. J. Uilenreef, Y. V. Nazarov, N. C. van der Vaart, and L. P. Kouwenhoven, *Changes in the magnetization of a double quantum dot*, Phys. Rev. Lett. **80**, 4951 (1998).

[52] A. V. Khaetskii and Y. V. Nazarov, *Spin relaxation in semiconductor quantum dots*, Phys. Rev. B **61**, 12639 (2000).

[53] T. Fujisawa, D. G. Austing, Y. Tokura, Y. Hirayama, and S. Tarucha, *Allowed and forbidden transitions in artificial hydrogen and helium atoms*, Nature **419**, 278 (2002).

[54] V. Fock, *Bemerkung zur Quantelung des Harmonischen Oszillators im Magnetfeld*, Zeitschrift für Physik **47**, 446 (1928).

[55] C. G. Darwin, *The diamagnetism of the free electron*, Proc. Cambridge Phil. Soc. **27**, 86 (1930).

[56] M. Taut, *Two electrons in a homogeneous magnetic field: particular analytical solutions*, J. of Phys. A **27**, 1045 (1994).

[57] C. Cohen-Tannoudji, B. Diu, and F. Laloë, *Quantum Mechanics, volume two* (Wiley, 1977).

[58] S. Siljamäki, *Wave function methods for quantum dots in magnetic field*, Doctoral dissertation, Helsinki University of Technology (2003), http://lib.tkk.fi/Diss/2003/isbn9512267047/.

[59] A. Harju, *Interacting electrons in a quantum dot: quantum Monte Carlo studies*, Doctoral dissertation, Helsinki University of Technology (1999).

[60] S. Siljamäki, A. Harju, E. Räsänen, J. Suorsa, and R. M. Nieminen, *Diagonalizations on a correlated basis*, Physica E **26**, 441 (2005).

[61] P. Hohenberg and W. Kohn, *Inhomogeneous electron gas*, Physical Review **136**, B864 (1964).

[62] W. Kohn and L. J. Sham, *Self-consistent equations including exchange and correlation effects*, Physical Review **140**, A1133 (1965).

[63] W. J. Hehre, L. Random, P. v. R. Schleyer, and J. A. Pople, *Ab initio molecular orbital theory* (John Wiley & Sons, New York, 1996).

[64] H. Saarikoski, *Density-functional approaches to interacting electrons in quantum dots*, Doctoral dissertation, Helsinki University of Technology (2003), http://lib.tkk.fi/Diss/2003/isbn9512267098/.

[65] E. Räsänen, *Electronic properties of non-circular quantum dots*, Doctoral dissertation, Helsinki University of Technology (2004), http://lib.tkk.fi/Diss/2004/isbn951227101X/.

[66] A. Harju, E. Räsänen, H. Saarikoski, M. J. Puska, and R. M. Nieminen, *Broken symmetry in density-functional theory: Analysis and cure*, Phys. Rev. B **69**, 153101 (2004).

[67] M. Helle, E. Räsänen, A. Harju, and R. van Leeuwen, *Exchange-correlation potentials in a two-electron quantum dot: Comparisons of local density approximation and exact potentials* (unpublished).

[68] A. Harju, S. Siljamäki, and R. M. Nieminen, *Two-electron quantum dot molecule: Composite particles and the spin phase diagram*, Phys. Rev. Lett. **88**, 226804 (2002).

[69] B. Szafran, F. M. Peeters, and S. Bednarek, *Exchange energy tuned by asymmetry in artificial molecules*, Phys. Rev. B **70**, 205318 (2004).

[70] B. Szafran and F. M. Peeters, *Three electrons in laterally coupled quantum dots: Tunnel vs electrostatic coupling, ground-state symmetry, and interdot correlations*, Phys. Rev. B **71**, 245314 (2005).

[71] V. W. Scarola and S. D. Sarma, *Exchange gate in solid-state spin-quantum computation: The applicability of the Heisenberg model*, Phys. Rev. A **71**, 032340 (2005).

[72] P. S. Drouvelis, P. Schmelcher, and F. K. Diakonos, *Global view on the electronic properties of two-electron anisotropic quantum dots*, Phys. Rev. B **69**, 035333 (2004).

[73] P. S. Drouvelis, P. Schmelcher, and F. K. Diakonos, *Probing the shape of quantum dots with magnetic fields*, Phys. Rev. B **69**, 155312 (2004).

[74] E. Räsänen, A. Harju, M. J. Puska, and R. M. Nieminen, *Rectangular quantum dots in high magnetic fields*, Phys. Rev. B **69**, 165309 (2004).

[75] R. Ugajin, *Stark effect on the spin-singlet-spin-triplet transition in a square-well quantum dot*, Physica B **253**, 92 (1998).

[76] B. Szafran, F. M. Peeters, S. Bednarek, and J. Adamowski, *Anisotropic quantum dots: Correspondence between quantum and classical Wigner molecules, parity symmetry, and broken-symmetry states*, Phys. Rev. B **69**, 125344 (2004).

[77] E. Räsänen, J. Könemann, R. J. Haug, M. J. Puska, and R. M. Nieminen, *Impurity effects in quantum dots: Toward quantitative modeling*, Phys. Rev. B **70**, 115308 (2004).

[78] E. Räsänen, H. Saarikoski, M. J. Puska, and R. M. Nieminen, *Electronic structure of rectangular quantum dots*, Phys. Rev. B **67**, 235307 (2003).

[79] J. Schliemann, D. Loss, and A. H. MacDonald, *Double-occupancy errors, adiabaticity, and entanglement of spin qubits in quantum dots*, Phys. Rev. B **63**, 085311 (2001).

[80] H. Saarikoski, A. Harju, M. J. Puska, and R. M. Nieminen, *Vortex clusters in quantum dots*, Phys. Rev. Lett. **93**, 116802 (2004).

[81] R. B. Laughlin, *Quantized Hall conductivity in two dimensions*, Phys. Rev. B **23**, 5632 (1981).

[82] J. K. Jain and T. Kawamura, *Composite fermions in quantum dots*, Europhys. Lett. **29**, 321 (1995).

[83] T. Chakraborty, V. Halonen, and P. Pietiläinen, *Magneto-optical transitions and level crossings in a Coulomb-coupled pair of quantum dots*, Phys. Rev. B **43**, 14289 (1991).

[84] D. Pfannkuche and R. R. Gerhardts, *Quantum-dot helium: Effects of deviations from a parabolic confinement potential*, Phys. Rev. B **44**, 13132 (1991).

[85] A. V. Madhav and T. Chakraborty, *Electronic properties of anisotropic quantum dots in a magnetic field*, Phys. Rev. B **49**, 8163 (1994).

[86] I. Magnúsdóttir and V. Gudmundsson, *Influence of the shape of quantum dots on their far-infrared absorption*, Phys. Rev. B **60**, 16591 (1999).

[87] C. A. Ullrich and G. Vignale, *Collective charge-density excitations of non-circular quantum dots in a magnetic field*, Phys. Rev. B **61**, 2729 (2000).

[88] V. Gudmundsson, A. Manolescu, R. Krahne, and D. Heitmann, *Nano-Physics and Bio-Electronics: A New Odyssey* (Elsevier, New York, 2002), chap. From single dots to interacting arrays.

[89] T. Chakraborty and P. Pietiläinen, *Optical signatures of spin-orbit interaction effects in a parabolic quantum dot*, Phys. Rev. Lett. **95**, 136603 (2005).

[90] J. Z. García, P. Pietiläinen, and P. Hyvönen, *Donor centers and absorption spectra in quantum dots*, Phys. Rev. B **66**, 195324 (2002).

[91] M. Koskinen, M. Manninen, and S. M. Reimann, *Hund's rules and spin density waves in quantum dots*, Phys. Rev. Lett. **79**, 1389 (1997).

[92] R. Egger, W. Häusler, C. H. Mak, and H. Grabert, *Crossover from Fermi liquid to Wigner molecule behaviour in quantum dots*, Phys. Rev. Lett. **82**, 3320 (1999).

[93] C. E. Creffield, W. Häusler, J. H. Jefferson, and S. Sakar, *Interacting electrons in polygonal quantum dots*, Phys. Rev. B **59**, 10719 (1999).

[94] P. A. Maksym, H. Imamura, G. P. Mallon, and H. Aoki, *Molecular aspects of electron correlation in quantum dots*, J. Phys.: Condens. Matter **12**, R299 (2000).

[95] S. M. Reimann, M. Koskinen, and M. Manninen, *Formation of Wigner molecules in small quantum dots*, Phys. Rev. B **62**, 8108 (2000).

[96] B. Reusch, W. Häusler, and H. Grabert, *Wigner molecules in quantum dots*, Phys. Rev. B **63**, 113313 (2001).

[97] A. Harju, S. Siljamäki, and R. M. Nieminen, *Wigner molecules in quantum dots: A quantum Monte Carlo study*, Phys. Rev. B **65**, 075309 (2002).

[98] E. Räsänen, H. Saarikoski, M. J. Puska, and R. M. Nieminen, *Wigner molecules in polygonal quantum dots: A density-functional study*, Phys. Rev. B **67**, 035326 (2003).

[99] B. Szafran, S. Bednarek, J. Adamowski, M. Tavernier, E. Anisimovas, and F. Peeters, *Accuracy of the Hartree-Fock method for Wigner molecules at high magnetic fields*, Eur. Phys. J. D **28**, 373 (2004).

[100] F. Bolton and U. Rössler, *Classical model of a Wigner crystal in a quantum dot*, Superlattices and Microstructures **13**, 139 (1993).

[101] F. Bolton, *Wenig-Electronen-Systeme in Quanten-Dots*, Ph.D. thesis, Universität Regensburg (1994).

[102] V. M. Bedanov and F. M. Peeters, *Ordering and phase transitions of charged particles in a classical finite two-dimensional system*, Phys. Rev. B **49**, 2667 (1994).

[103] B. Partoens, V. Schweigert, and F. Peeters, *Classical double-layer atoms: artificial molecules*, Phys. Rev. Lett. **79**, 3990 (1997).

[104] N. Metropolis, A. W. Rosenbluth, M. N. Rosenbluth, A. H. Teller, and E. Teller, *Equation of state calculations by fast computing machines*, J. of Chem. Phys. **21**, 1087 (1953).